REPORT OF INVESTIGATIONS/1995

Hazards of Conveyor Belt Fires

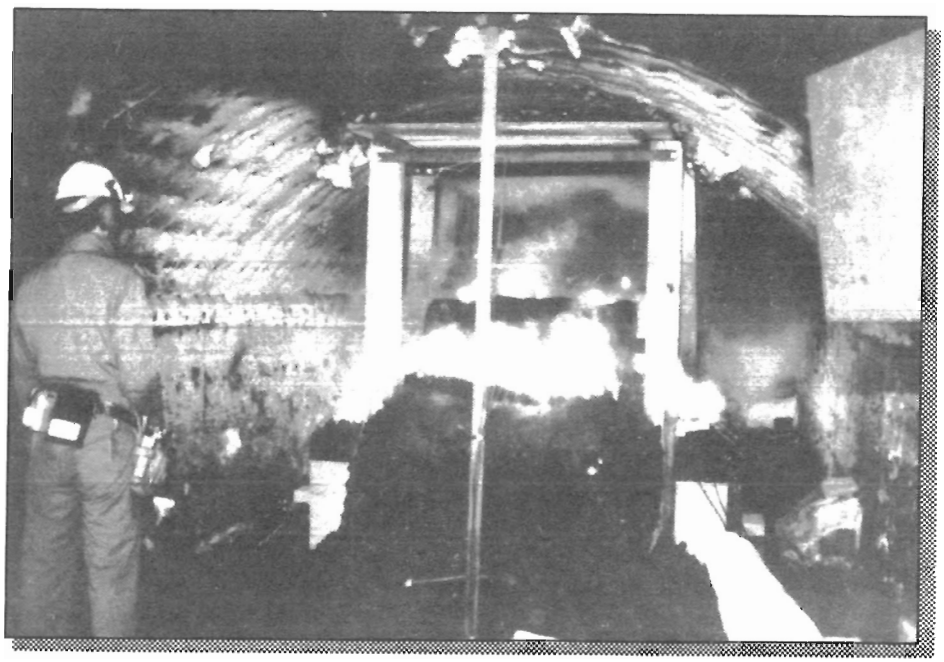

UNITED STATES DEPARTMENT OF THE INTERIOR

UNITED STATES BUREAU OF MINES

U.S. Department of the Interior
Mission Statement

As the Nation's principal conservation agency, the Department of the Interior has responsibility for most of our nationally–owned public lands and natural resources. This includes fostering sound use of our land and water resources; protecting our fish, wildlife, and biological diversity; preserving the environmental and cultural values of our national parks and historical places; and providing for the enjoyment of life through outdoor recreation. The Department assesses our energy and mineral resources and works to ensure that their development is in the best interests of all our people by encouraging stewardship and citizen participation in their care. The Department also has a major responsibility for American Indian reservation communities and for people who live in island territories under U.S. administration.

Cover: Large-scale gallery fire involving coal and conveyor belting.

Report of Investigations 9570

Hazards of Conveyor Belt Fires

By Frank J. Perzak, Charles D. Litton,
Kenneth E. Mura, and Charles P. Lazzara

UNITED STATES DEPARTMENT OF THE INTERIOR
Bruce Babbitt, Secretary

BUREAU OF MINES
Rhea Lydia Graham, Director

International Standard Serial Number
ISSN 1066-5552

CONTENTS

ILLUSTRATIONS

TABLES

TABLES—Continued

UNIT OF MEASURE ABBREVIATIONS USED IN THIS REPORT

A	ampere
cm	centimeter
cm/h	centimeter per hour
cm/s	centimeter per second
g/g	gram per gram
g/m^2	gram per meter squared
g/m^2s	gram per meter squared per second
g/m^3	gram per cubic meter
g/s	gram per second
h	hour
J/g·K	joule per gram per kelvin
kg/m^2	kilogram per square meter
kg/m^3	kilogram per cubic meter
kJ/g	kilojoule per gram
kJ/(g·°C)	kilojoule per gram per degree Celsius
kJ/m	kilojoule per meter
kJ/(m·s·°C)	kilojoule per meter per second per degree Celsius
kJ/m^3	kilojoule per cubic meter
kJ/s	kilojoule per second
kW	kilowatt
kW/min	kilowatt per minute
L/min	liter per minute
m	meter
m/s	meter per second
m^{-1}	inverse meter
m^2	square meter
m^2/g	square meter per gram
m^3/kJ	cubic meter per kilojoule
m^3/min	cubic meter per minute
m^3/s	cubic meter per second
m^4/kJ	quartic meter per kilojoule
min	minute
mm	millimeter
MW	megawatt
ppm	part per million
s	second
V	volt
W	watt
°C	degree Celsius

Reference to specific products does not imply endorsement by the U.S. Bureau of Mines.

HAZARDS OF CONVEYOR BELT FIRES

By Frank J. Perzak,[1] Charles D. Litton,[2] Kenneth E. Mura,[3] and Charles P. Lazzara[4]

ABSTRACT

This report describes a U.S. Bureau of Mines study on the hazards of large-scale conveyor belt fires in underground coal mines, as a function of both air velocity and distance from belt surface to gallery roof. The fire hazards considered were smoke obscuration, toxic effects of carbon monoxide (CO), and elevated air temperatures downstream of the fire. All of these hazards scale with the ratio of fire intensity to ventilation airflow. These hazards were all found to be greater at the lower belt-to-roof distance, owing to the greater fire intensities that resulted. The hazards of smoke obscuration and elevated CO levels were greater at lower air velocities.

Smoke obscuration was found to be the earliest hazard, reaching critical levels before the stage of belt flame spread. Critical levels of CO and downstream air temperatures were not reached until the later stages of flame spread. Fire growth rates during rapid flame spread were much greater than rates measured during the early stages of belt burning.

Data were analyzed to determine the early-warning capability of fire sensors. Smoke sensors provided the earliest warning, followed closely by CO sensors. Thermal sensors did not exhibit any early warning capability.

[1]Research chemist.
[2]Research physicist.
[3]Physical science technician.
[4]Supervisory research chemist.
Pittsburgh Research Center, U.S. Bureau of Mines, Pittsburgh, PA.

INTRODUCTION

Conveyor belt entries in underground coal mines are areas where the risk of fire is high. About one-third of all reported coal mine fires from 1978 to 1992 occurred in belt entries (*1*).[5] These fires typically originate from the contact of loose coal with overheated equipment, such as stuck idlers or slipping drive drums. The sustained contact of the loose coal with these hot objects produces smoldering of the coal that can be followed by ignition of the coal, producing open flame. Once the transition to coal flame has occurred, the developing fire begins to increase in intensity and, in many cases, will eventually ignite the conveyor belt. When the conveyor belt becomes involved in the fire, the fire intensity begins to increase at a more rapid rate. If the conveyor belt has poor flame resistance, the flames will begin to spread along the exposed surfaces of the belt and will eventually ignite the coal roof and rib.

As the developing fire progresses from one stage to the next, the hazard level also increases. In terms of human safety, the hazards are primarily due to insufficient warning time regarding the high levels of carbon monoxide (CO), other toxic gases, and smoke that are produced. During the latter stages of fire growth, heat generated by the fire also becomes a major concern. Of the smoke and gas hazards, it is generally recognized that smoke represents the earliest impediment to miner safety because of the severe reduction in visibility. Significant visibility reductions can also occur during the burning of loose coal. As the fire progresses into stages of belt involvement and spreads to other combustibles within the belt entry, the concentrations of CO and other toxic gases increase to dangerous and potentially lethal levels.

The stages of flame spread along the conveyor belt and to other combustibles have the greatest potential for property damage. Data on the magnitudes of these hazards, as well as the potential of the fire to spread to other combustibles, are scarce because of the size of the fires and the scale of the experiments that must be performed to address these questions. Previous work (*2*) summarizes some of the interactive problems of combustion, detection, and fire growth in mine fires.

It is the intent of this report to provide some answers to these questions based on experiments conducted in a large-scale fire gallery. In these experiments, the levels of CO, carbon dioxide (CO_2), and heat produced during the stages of flame spread along the belt and along a wooden roof were studied and quantified. The earliest detection times by CO, smoke, and thermal sensors were studied at various airflows. The propensity of the fire to spread to a wooden roof and the contributions of the fire involvement of the roof to the overall hazard were examined primarily as a function of the air velocity and the belt-to-roof distance. A wooden roof was used in this study since it is easier to install than a coal roof and it is more easily ignited. The resulting data provide significant insight into the hazards of propagating mine fires and their detection in conveyor belt entries, and the complex role that ventilation plays in the total process.

In a previous U.S. Bureau of Mines (USBM) report (*3*), a series of large-scale experiments was described and the data were used to develop guidelines for the detection of fires in conveyor belt entries by CO and smoke sensors. The effectiveness of the developed guidelines are addressed in a section entitled "Fire Detection," which precedes the analysis of the test data of this report. The current data are analyzed primarily in terms of the hazards resulting from the various stages of flame spread and the effect of ventilation. This work was done as part of the USBM program to enhance mine safety.

EXPERIMENTAL DESIGN

FIRE GALLERY DESCRIPTION

The large-scale experiments were conducted at the USBM's Lake Lynn Laboratory fire gallery. The aboveground fire gallery is a 27.4-m-long tunnel constructed of masonry block walls, a steel arch roof, and a concrete floor. The tunnel ventilation is provided by a 1.83-m-diam, 3,500 m^3/min fan mounted in a 6.1-m-long tapered transition section. Ventilation flow can be adjusted by changing the pitch of the fan blades and/or by throttling the fan intake. A schematic of the fire gallery is shown in figure 1. The cross-sectional area of the tunnel is 7.53 m^2. The interior walls and roof are covered with ceramic blanket insulation. All tunnel distances are measured from the junction of the fire tunnel and transition section, designated as the 0-m mark. A conveyor frame, approximately 21.3 m long by 1.52 m wide, is centered in the tunnel. The frame has a 0.46-m-diam tail pulley and 0.13-m-diam troughed idler assemblies spaced at 1.23-m intervals.

[5]Italic numbers in parentheses refer to items in the list of references preceding the appendixes.

Figure 1

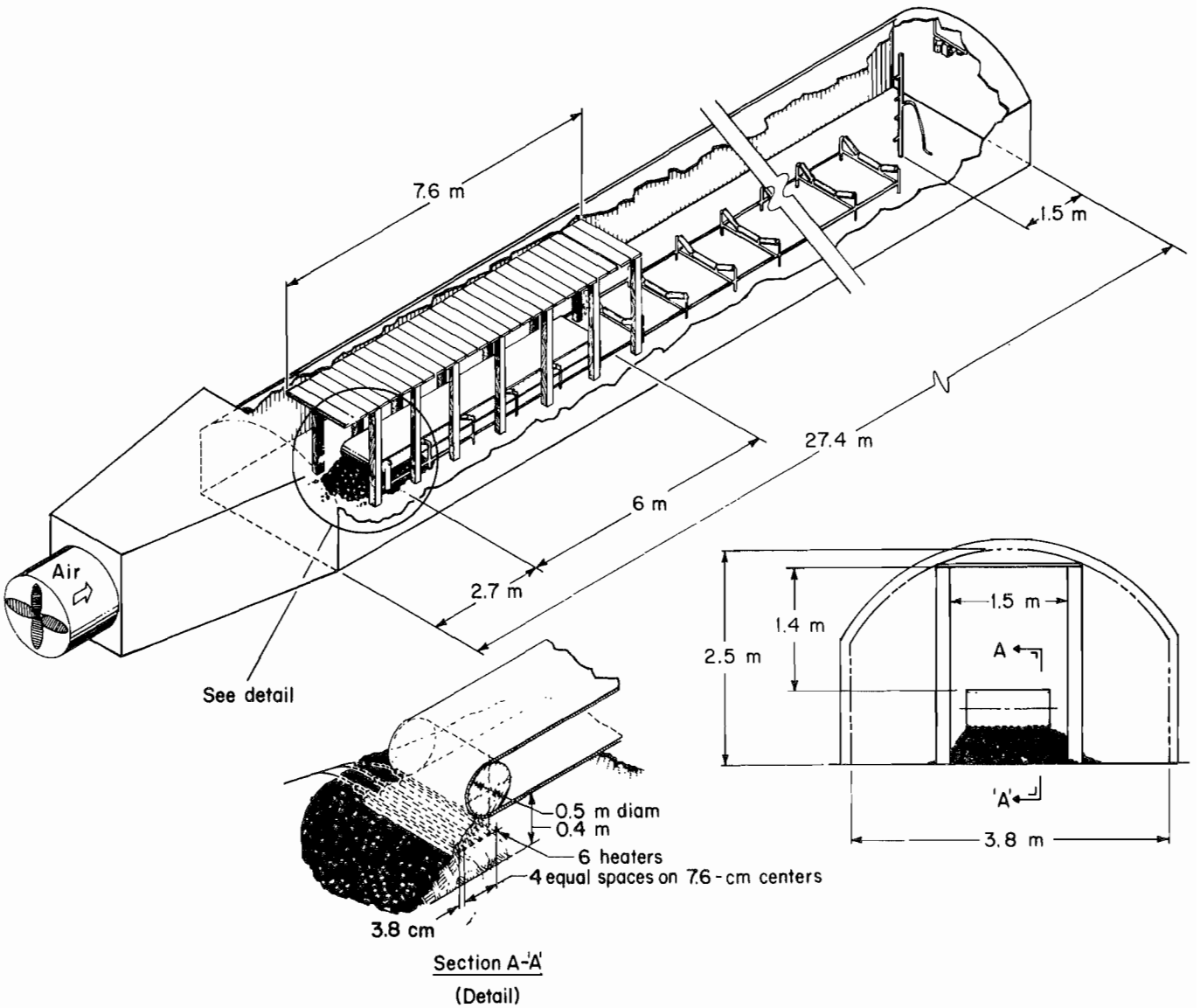

Schematic view of experiment: coal pile, belting, and wood roof structure in fire gallery, showing heater pipe igniters (section A-'A') in coal pile and the 1.4-m belt-to-roof separation.

COAL PILE CONFIGURATION

A coal pile fire, located just upstream and directly below the tail pulley, was the ignition source for the tests. The trapezoidal-shaped coal pile, measuring 0.41 m deep by 2.13 m long by 2.0 m wide, consisted of run-of-mine Pittsburgh coal (two different batches) or Sewickley nut coal (nominally 5 cm and smaller). The top surface of the coal pile was 1.5 m long (along the length of the conveyor structure) by 1.1 m wide. The coal fire was started with six electrical strip heaters placed inside seamless black pipes positioned 15 cm below the top surface of the coal pile. Each strip heater was 1.9 cm wide by 103.5 cm long, with a heated length of 94.3 cm, and was rated at 2,100 W at 240 V. The black seamless pipe was 2.67 cm OD by 2.34 cm ID by 101.6 cm long. The strip-pipe heaters were spaced with centers 7.6 cm apart except for the first heater spacing, which was 3.8 cm, as shown in figure 1. Stainless steel sheathed type K thermocouples were attached to three of the six pipes to monitor their temperatures. The

voltage to the strip heaters was controlled by two variable transformers, with three strip heaters on each transformer.

The heater voltages were maintained as follows: 0 to 30 min, 50 V; 30 to 45 min, 100 V; 45 to 120 min, 150 V; 120 min to heater failure or shutoff, 200 V. In early tests, three heaters were connected in parallel on two separate 30-A circuits. Loss of only one heater through shorting would result in losing half the heating power. Later tests used six heaters on separate 10-A circuits that allowed the remaining heaters to operate in the event of any individual heater failure. The heaters were turned off only after the coal and belt fire was well developed in the ignition area.

The temperatures through the coal pile were determined by thermocouples in the coal pile at the same height as the heaters. Five stainless steel sheathed type K thermocouples were positioned 15 cm below the belt-coal interface at several places. Three of the thermocouples were centered at 15, 31, and 122 cm from the last strip-pipe heater under the tail pulley. The other two thermocouples were 31 cm from the tail pulley and about 15 cm from the side edges of the coal pile.

CONVEYOR BELT AND BELT THERMOCOUPLE CONFIGURATION

The conveyor belt was a styrene-butadiene rubber (SBR) belt that passed the Federal acceptance test (*4*) with a flameout time of less than 22 s. An average flameout time of less than 1 min is sufficient to pass this test. The 1.07-m-wide, three-ply belt was about 11 mm thick, with a top cover thickness of 5 mm and a bottom cover thickness of about 2 mm. The belt weighed 14.0 kg/m^2. A 12.8-m length of the conveyor belting, with top cover side up, was placed on the gallery belt structure, stretched around the tail pulley and over the top and bottom idler pulleys, and fastened to the conveyor structure at its downstream ends. The bottom strand of belting rested on top of the coal pile. The exposed area of the top belt's upper surface was about 6.52 m^2. The distance from the bottom belt to the upper belt was about 0.46 m, and the distance from the top belt's upper surface to the wood roof was either 1.4 m (figure 1), or 0.80 m, measured from the center of the belt trough. The closer belt-to-roof separations were achieved by fixing the wood roof height in the fire gallery and raising the conveyor structure and coal pile on 0.61-m-high concrete blocks.

Thermocouples were embedded just below the belt surfaces about 1.2 m apart along the upper and lower surfaces of both the top and bottom strands of belting. Additionally, a 0.64-cm-diam stainless steel sheathed thermocouple was positioned at the coal-belt interface under the tail pulley. These thermocouples were used to determine the fire spread away from the ignition area and the flame spread rate along the belt.

WOOD ROOF CONFIGURATION

A wooden roof was used instead of a coal roof because it was easier to implement experimentally. Wood is more readily ignited than coal because of its lower surface ignition temperature and heat capacity, and thus it represents a more severe hazard in a fire. Wood is also likely to be present in many mine areas where roof support is necessary.

For these tests a timber-supported wood plank roof, 7.62 m long by 1.8 m wide (13.72 m^2), was constructed, starting about 0.92 m upstream of the tail pulley. The wood roof provided additional fuel during belt flame spread, which increased the severity of the fire. The 14 timbers and 25 roof planks were nominal 15.4-cm-square by 2.3-m-long hardwood timbers and nominal 2.5-cm-thick by 30.5-cm-wide by 1.8-m-long red oak planks, respectively. Seven roof support timbers were spaced 1.3 m apart on each side of the conveyor structure for a distance of 7.62 m (figure 1).

TUNNEL AIRFLOW

The airflow over the belt sample was adjusted prior to the start of a test to within 10% of the desired value, 0.76, 1.52, or 4.06 m/s, based on measurements made with a handheld anemometer. The measurements were taken at several locations along the length of the belt sample, between the top belt and wood roof, and the values were averaged. The airflow was also measured at about 12 points near the exit plane of the tunnel. The average exit airflow was about 20% lower than the airflow over the belting because of the larger, unobstructed cross-sectional area near the exit. The average tunnel exit airflow is designated V_e, and the average airflow over the belt sample is designated V_0.

TUNNEL THERMOCOUPLES AND GAS-SAMPLING PROBES

An array of 12 thermocouples was positioned over the tunnel cross section at 24.4 m to measure the exit gas temperatures. Type K 20-gauge bare-bead thermocouples were placed through the top of the roof planks flush with the lower plank surface, 1.52 m apart along the centerline of the roof, starting with the first plank and ending with the last. Three air thermocouples were spaced 3.7 m apart and 5 cm below the wood roof along its centerline, starting at the first plank. Several type K thermocouples were

spaced 6.1 m apart, 15 cm from the roof, starting at the gallery entrance (0.0-m position) and ending at the gallery exit (27.4 m).

A gas-sampling probe was placed at 25.9 m, about 23.5 m downstream of the coal fire. The gas probe consisted of a nominal 5-cm-diam steel pipe with four inlet ports, 0.31 cm in diam, spaced 48.8 cm apart along the 2.5-m vertical tunnel axis. The gas-sampling line was 1.3-cm-diam by about 18.3-m-long copper and polyethylene plastic tubing. The gases were drawn into the probe by a 17-L/min displacement pump and exhausted into infrared absorption and chemical cells for continuous on-line analysis of CO, CO_2, and oxygen (O_2). The various gas-specific analyzers were calibrated prior to each test and checked using grab samples during the test. The grab samples were analyzed by gas chromatography.

In the earlier tests, tests 1 to 14, the smoke was sampled along with the gases and monitored using continuous pumped ionization smoke detectors. In later tests, tests 15 and 16, a separate smoke-sampling probe was positioned near the gas probe at 24.4 m. The smoke probe consisted of a nominal 2.54-cm-diam steel pipe with four inlet ports, 0.229-cm diam, spaced 48.8 cm apart. The smoke was drawn through a 1.2-cm-diam line 4.6 m long directly into a commercial ionization smoke detector. For all the tests, a commercial diffusion-convective ionization smoke detector was located a nominal 0.43 m down from the roof at the 26.5-m tunnel position (0.91 m from the tunnel exit). The time for the smoke alarm was determined by averaging the alarm times of the two smoke detectors.

DATA ACQUISITION

The outputs of all the thermocouples and the gas and smoke analyzers were connected to two 48-channel microprocessors for transmission to a VAX computer for storage. The data were collected every 5 s and displayed on computer terminals. After the test, time-temperature, gas concentration, and smoke plots were retrieved from storage for analysis.

During the tests, the times to coal smoke, coal flames, and belt flames were recorded. The experiments were also recorded on videotape, and strip-chart recordings were made of the gas analyzer outputs.

RESULTS

INITIAL COAL PILE SMOLDERING AND FIRE GROWTH RATES

Because of the slow spread rate for coal smoldering and the good insulation properties of the coal, only the closest centered thermocouple, 15 cm downstream of the nearest heater, reached 200 °C in any of these tests. The propagation rates for coal pile smoldering were less than 6 cm/h in this test series. As a result, the average time of smoldering, measured from the time of first visible smoke until the time that flames were observed on the coal pile, was 66.3 ± 18.4 min.

An earlier USBM study presented data (equation 7 of reference 3) on the coal fire growth rates prior to ignition of the conveyor belt as a function of the air velocity. Coal fire growth rates measured during these tests were in good agreement with the previous data.

FIRE DETECTION

In this section, the results of previous work (*3*) for CO and smoke sensors are applied to these test data. To do this, the average gas and smoke concentrations measured 23.5 m downstream of the coal fire are assumed to be the same as those measured by a sensor 305 m downstream of the fire where the gases and smoke are completely mixed. The cross-sectional area of the fire gallery is assumed constant at 7.53 m^2, and only the average air velocity (V_e) in the fire gallery is changed.

Using the nomographs for CO and smoke sensors at 305-m spacing (figures 7 and 8, respectively, reference 3), column 4 of table 1 indicates the CO alarm (CO_A) level above ambient that should be used for each test at the various airflows. For airflows lower than 1.4 m/s, the CO_A levels should be 10 ppm, or less. At higher airflows, the CO_A levels range from 5 to 7 ppm depending on the actual air velocity. The CO_A level for test 11 was 6 ppm, using the nomograph in figure 7 of reference 3; however, three of six electrical heaters shorted at 164 min. Therefore, only 5 ppm CO was achieved at 142.7 min.

Coal Ignition

Successful fire detection by sensors, using the criterion of reference 3, is detection of the small coal fire within 14.25 min after flaming so that the conveyor belting has not yet been ignited. The elapsed times (Δt_X), from coal ignition time (t_{CI}) until sensor alarm time [$(t_A)_X$] offset by 14.25 min, were calculated from the experimental CO and smoke concentrations and the thermal sensor temperatures

in these tests. The averages from all these tests are also given in appendix E. The thermal detection time approximately equals the thermal alarm time $(t_A)_T$ since the sum of the transport time plus the thermal response time is less than 1/2 min. Thermal detector spacings are typically on the order of several meters.

The coal ignition time is defined as the interval from the start of electrical heating until the occurrence of visible flaming above the coal pile. The coal ignition time can also be determined from the time when a sudden increase in the level of CO_2 occurs simultaneously with a decrease in the CO level. Column 4 of table 1 gives the CO alarm (CO_A) level and column 5 the elapsed time available (Δt_X) in minutes after detection by the CO sensor and before the coal flaming will potentially ignite the conveyor belting. A negative time value for Δt_X indicates that the coal fire was not detected prior to belt ignition (e.g., tests 1 and 10). The larger the negative value, the poorer the system's performance. Conversely, a positive time difference indicates that the system was effective, and the larger the positive value, the better the system's performance.

With the exception of two tests, all CO elapsed times in column 5 of table 1 were positive. The experimental overall average CO alarm ($(t_A)_{CO}$ = 131±20 min, appendix E) occurred 27±20 min before the overall average belt ignition (t_{BI} = 158±19 min, appendix E) with no significant effect (within one standard deviation) of airflow changes from 0.7 to 4.0 m/s. Tests 1 and 10 gave only a 10-min and 4-min early-warning time to potential belt ignition, respectively. The overall success rate of the CO sensor criterion was about 88% (2 failures in 16 trials).

Table 1.—Coal ignition times (t_{CI}), CO alarm levels (CO_A), and elapsed times (Δt_X) for CO, smoke (D), and thermal (T) sensors at various airflows (V_e)

Test	V_e, m/s	t_{CI}, min	CO_A,[1] ppm	Δt_X,[2] min		
				CO	D	T
			LOW AIRFLOW			
3	0.68	147	10	44.5	63.4	-68.8
4	0.73	130	10	14.7	63.7	-53.8
8	0.67	153	10	38.5	29.4	ND
9	0.67	128	10	14.5	19.9	ND
12	0.74	133	10	16.5	39.0	-17.8
14	0.62	128	10	24.1	33.6	-28.8
16	0.64	138	10	32.3	52.3	-32.0
Av	0.68±0.04	137±10	10	26±12	43±17	NAp
			MEDIUM AIRFLOW			
1	1.3	124	10	-3.7	19.9	-17.8
7	1.4	139	10	21.4	24.4	-2.8
15	1.2	156	10	41.2	53.7	-62.8
Av	1.3±0.1	140±16	10	20±23	33±18	< -28
			HIGH AIRFLOW			
2	2.8	118	7	3.4	16.4	-12.8
5	3.1	111	6	9.5	5.5	ND
6	3.7	123	5	7.6	13.6	-9.8
10	3.4	122	6	-10.5	13.1	-88.8
11[3]	3.5	152	[3]5	23.6	13.6	ND
13	2.7	134	7	15.4	22.4	-18.8
Av	3.2±0.4	127±15	NAp	8.2±12	14±5	NAp
Av over all airflows		134±13	NAp	18±16	30±19	NAp

Av Arithmetic average and standard deviation.
NAp Not applicable.
ND Not detected because of early heater failure and lack of flame propagation on wood roof.
[1]Constraints on CO alarm levels using criterion of reference 3 at 305-m spacing.
[2]Elapsed time from coal ignition until X sensor alarm time $[(t_A)_X]$, offset by 14.25 min. Defined by $\Delta t_X \equiv t_{CI} - (t_A)_X + 14.25$ min, where X is CO, D, or T.
[3]Three heaters failed at 164 min; using a CO_A value of 5 ppm gives the positive value.

The calculated elapsed times for smoke detection are similarly given in column 6 of table 1. The alarm times of the two smoke detectors were averaged to determine smoke alarm times. Detection of coal ignition occurred 30±19 min before belt ignition with little effect due to airflow changes from 0.7 to 4.0 m/s. The smoke sensors responded 12 min earlier, on the average, than the CO sensors and had a 100% success rate for meeting the criterion of reference 3.

In addition, a similar analysis was made for point-type heat sensors (PTHS's), which are still the most widely used sensors for fire detection along conveyor belt entries. Although PTHS's were not used in these tests, the downstream air temperature near the roof of the tunnel at a distance of 7.6 m from the fire origin was recorded every 5 s. By using the standard minimum temperature of 57.2 °C as the alarm point for a PTHS, it is possible to determine the time differences between coal ignition and thermal alarm times. The thermal alarm elapsed times with respect to coal ignition are given in column 7 of table 1. The PTHS was singularly ineffective compared with either the CO or the smoke sensors. All the elapsed times were negative, ranging from a low value of "not detected," for the belt fires that did not grow, to the best value of -2.8 min. In contrast, 88% of the time differences for the CO sensors were positive, ranging from a low value of −10.5 min to the best value of 44.5 min. All the time differences for the smoke sensors were positive, ranging from a low value of 5.5 min to the best value of 63.7 min.

The averaged sensor response times for both the CO and smoke alarms in table 1 varied inversely with the flow rate, as expected from simple contaminant dilution and mixing with air. On the average, the CO and smoke sensors downstream of the heated coal pile gave an early warning of the coal fire breakout from the smoldering stage to flaming at both the low and medium airflows. At the low airflows, the CO sensors on the average gave about a 12-min (26 minus 14.25 min) warning of the coal fire flaming, and the smoke sensors gave about a 29-min warning. At the high airflow, only the smoke sensors gave on the average an advance warning of the coal fire flames. However, at the high airflow even the smoke sensors gave no warning of the incipient coal flame in two tests (5 and 10).

Belt Ignition

Fire detection prior to conveyor belt ignition is one of the prime concerns in evaluating the available escape time from a mine fire because of the possible rapid flame spread on the belt once the fire reaches a critical size. However, the exact time of belt ignition is not known as precisely (±5 min) as the time of coal ignition (±0.5 min), since abrupt changes in the CO_2 and CO levels did not occur at belt ignition. Additionally, it was difficult to visually determine the time of belt ignition because of smoke obscuration.

The CO alarm time, referenced to the estimated belt ignition time (t_{BI}), was calculated at the CO alarm levels given in column 4 of table 2, as was done for table 1. The resulting belt ignition times minus the sensor alarm times are given in columns 5, 6, and 7 of table 2 for CO, smoke, and thermal sensors, respectively. As in table 1, the effectiveness of the detection system can be represented by large positive time differences. The CO sensors (except in test 1) and the smoke sensors were highly effective, whereas the thermal sensors were very ineffective. For the CO sensors (column 5 of table 2), the time differences ranged from a low value of −2.9 min to a high value of 55.2 min (test 5), with the total average of 28±18 min. All the time differences for smoke detectors were positive, ranging from a low value of 14.3 min (test 6) to a high value of 78.4 min (test 4), with the total average of 40±21 min. For the thermal sensor, the time differences were all negative, ranging from a low value of "not detected" to a high value of −11 min.

The effect of airflow on the elapsed time differences (Δt_X) in table 1 for CO and smoke is a trend toward shorter warning times at the higher airflows. The averaged times at each flow for the CO sensors in column 5 of table 1 were 26, 20, and 8.2 min at average exit airflows of 0.68, 1.3, and 3.2 m/s, respectively. The averaged values for the smoke sensors in column 6 of table 1 also show the same trend of shorter warning times with increasing airflow and were 43, 33, and 14 min at exit airflows of 0.68, 1.3, and 3.2 m/s, respectively. However, from table 2, the time differences between CO and smoke sensor alarms and belt ignition show no dependence on the air velocity.

Also from table 2, the average time that could be saved by replacing thermal sensors with CO sensors would be >62 min, with the added benefit that the fire would be detected before the belt ignited. Replacing thermal sensors with smoke sensors would on the average result in a >74-min time saving. There were four tests in which the fire was detected by both the CO and the smoke sensors but not by the thermal sensors. In three of these tests (tests 8, 9, and 11) the coal fire did not produce a belt flame spread because the heaters shorted out and the minimum energy for producing a propagating belt fire was not achieved during the 4-h test period. The remaining test (test 5) produced a belt flame spread that did not ignite the wood roof.

The average time difference between the belt ignition and coal ignition was 24±16 min in this study versus

17±9 min in the earlier study (using only the R11 data of table 4, reference 3), which used a different test configuration. The previously mentioned 14.25-min time difference between belt ignition and coal ignition included data from both non-fire-resistant belting and fire-resistant polyvinyl chloride and neoprene belting as well as the R11-type (SBR) belting. The approximately 7-min longer time interval for belt ignition from the start of the flaming coal in this study is also partially due to the more deeply buried heaters (15 cm versus 5 cm) and the smaller air gap between the coal pile and belting (0 cm versus 5 to 10 cm), both of which would tend to increase the coal and belt smoldering times.

INITIAL STAGES OF BELT FIRE GROWTH AND HEAT RELEASE RATES

For all practical purposes, the onset of significant hazards does not occur in this test scenario until the conveyor belt has ignited. Once the belt has ignited, the fire size begins to increase at a rapid rate, typically much faster than that of the initiating coal fire. The conveyor belt burns locally in the vicinity of the small coal fire until the total fire size is sufficient for belt flames to begin to spread downstream along the exposed belt surfaces.

Table 2.—Belt ignition times (t_{BI}), CO alarm levels (CO_A), and alarm times [$t_{BI} - (t_A)_X$] for CO, smoke (D), and thermal (T) sensors at various airflows (V_e)

Test	V_e, m/s	t_{BI}, min	CO_A,[1] ppm	$t_{BI} - (t_A)_X$,[2] min		
				CO	D	T
			LOW AIRFLOW			
3	0.68	160	10	43.2	62.1	−70
4	0.73	159	10	29.2	78.4	−39
8	0.67	162	10	33.2	24.1	ND
9	0.67	175	10	47.2	52.6	ND
12	0.74	140	10	9.7	32.2	−32
14	0.62	141	10	22.8	32.3	−43
16	0.64	145	10	25.0	45.0	−47
Av	0.68±0.04	155±13	10	30±13	47±19	NAp
			MEDIUM AIRFLOW			
1	1.3	139	10	−2.9	20.6	−17
7	1.4	163	10	31.1	34.1	−17
15	1.2	170	10	40.9	53.4	−63
Av	1.3±0.1	157±16	10	23±23	36±16	−32±27
			HIGH AIRFLOW			
2	2.8	134	7	5.1	18.1	−11
5	3.1	171	6	55.2	51.2	ND
6	3.7	138	5	8.3	14.3	−24
10	3.4	200	6	53.3	76.8	−25
11	3.5	182	[3]5	[3]39.3	[3]29.3	ND
13	2.7	142	7	9.1	16.1	−25
Av	3.2±0.4	161±27	NAp	28±24	34±25	NAp
Av over all airflows		158±19	NAp	28±18	40±21	NAp

Av Arithmetic average and standard deviation.
NAp Not applicable.
ND Not detected because of early heater failure and lack of flame propagation on wood roof.
[1]Constraints on CO alarm levels using the criterion of reference 3 at 305-m spacing.
[2]Alarm time relative to belt ignition = $t_{BI} - (t_A)_X$, where X is CO, D, or T.
[3] Three heaters failed at 164 min; using a CO_A value of 5 ppm gives the positive value.

The times from the start of the test to belt ignition (t_{BI}) and to the onset of spreading belt flames (t_{BFS}) and the heat release rates at the time of belt ignition (Q_{BI}) and at the time of belt flame spread (Q_{BFS}), averaged over 1 min, are given in table 3 for all of the tests that resulted in belt flame spread, including five tests from reference 3 (81A, 78, 85, 80, and 83). The calculations of the fire intensity or the heat release rates (Q) are described in appendix B, and their values are estimated using equation B-1.[6] The time difference ($t_{BFS} - t_{BI}$) between belt ignition and the onset of spreading belt flames is the time period of belt fire growth. The belt fire heat release rates at the time of belt ignition (Q_{BI}) and at the onset of belt flame spread (Q_{BFS}) at the local velocity (V_0) are given in columns 5 and 6 of table 3, respectively. The fire growth-rate parameter for SBR conveyor belt fires (α_{SBR}) during the time from belt ignition to start of belt flame spread is calculated from

$$\alpha_{SBR} = \frac{Q_{BFS} - Q_{BI}}{t_{BFS} - t_{BI}} \tag{1}$$

and is given in column 7 of table 3. The burning rate of the conveyor belt during this growth stage should depend only upon the local air velocity, all other things being equal. Consequently, the belt fire growth rates observed in these experiments were added to those of the previous experiments (R11 data from reference 3, table 5) so that the database was expanded. The average values of the initial belt fire growth rates at each air velocity can be expressed as

$$\alpha_{SBR} = 9.9\ V_0^{1.5}. \tag{2}$$

Figure 2 shows the experimental values of α_{SBR}, from column 7 of table 3, and a plot of equation 2 at the local air velocities (V_0).

The potentially greater fire hazards from larger values of the fire growth rates (α_{SBR}), which occur at higher velocities (equation 2), are mitigated by larger heat losses at the higher airflows. Larger heat release rates are needed to spread belt flames at the higher air velocities. An estimate of the time (Δt_{PRED}) that a small, localized SBR belt fire will burn before sufficient energy heats a critical mass of belt and flames begin to spread can be determined as follows. Let the heat release rate be referenced to that at belt ignition time and defined as

$$Q_{SBR}(t) - Q_{BI} \equiv \alpha_{SBR}\ (t - t_{BI}), \tag{3}$$

where t is any time after belt ignition. At the onset of belt flame spread,

$$Q_{SBR} = Q_{BFS}. \tag{4}$$

At each air velocity,

$$\Delta t_{PRED} \equiv t_{BFS} - t_{BI} = \frac{Q_{BFS} - Q_{BI}}{\alpha_{SBR}}. \tag{5}$$

The experimental heat release rates at the times of belt ignition and belt flame spread (table 3), normalized by the airflow (Q/V_0), are given in columns 2 and 3 of table 4, respectively. The calculated belt fire growth values (α_{SBR}) from equation 2 are given in column 4; the experimental values are in column 5. The average heat release rates normalized by the airflow are 27±11 and 394±180 kJ/m at the times for belt ignition and belt flame spread, respectively. The predicted elapsed times (Δt_{PRED}) for belt fire growth, from belt ignition to start of belt flame spread at each airflow, are given in column 2 of table 5 and were calculated by equation 5 as follows:

$$\Delta t_{PRED} = \frac{Q_{BFS} - Q_{BI}}{\alpha_{SBR}} = \frac{(394 - 27) \cdot V_0}{9.9\ V_0^{1.5}} = 37.1\ V_0^{-0.5}. \tag{6}$$

The experimental elapsed times (Δt_{EXPTL}) for belt fire growth, from belt ignition to the start of flame spread, are given in column 3 of table 5.

Figure 2

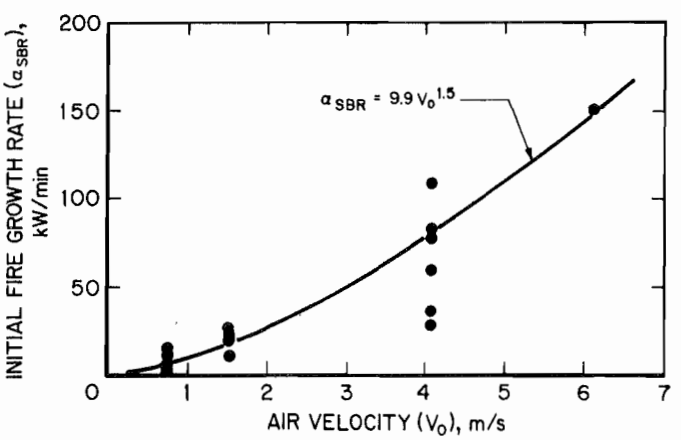

Experimental fire growth rate with respect to air velocity.

[6]Equation numbers with a B-prefix refer to equations in appendix B.

Table 3.—Times to belt ignition and belt flame spread (t_{BI} and t_{BFS}), their heat release rates (Q_{BI} and Q_{BFS}), and initial belt fire growth rates (α_{SBR}) at various local airflows (V_0)

Test	V_0, m/s	t_{BI}, min	t_{BFS}, min	Q_{BI}, kW	Q_{BFS}, kW	α_{SBR},[1] kW/min
			LOW AIRFLOW			
3	0.77	160	235	20	170	2.0
4	0.75	159	207	43	270	4.7
12	0.80	140	182	23	490	11
14	0.76	141	254	22	710	6.1
16	0.75	145	205	41	380	5.6
81A[2]	0.76	[2]8	[2]24	20	250	15
Av	0.77±0.02	149±10	217±28	28±11	378±198	7.4±4.7
			MEDIUM AIRFLOW			
7	1.5	163	184	40	450	20
15	1.7	170	233	54	720	11
78[2]	1.5	[2]26	[2]45	60	480	23
85[2]	1.5	[2]6	[2]23	30	490	27
Av	1.6±0.1	167±5	209±35	46±14	534±123	20±7
			HIGH AIRFLOW			
2	4.5	134	147	52	1,470	109
5	3.8	171	199	NA	1,670	≤60
6	4.0	138	163	32	2,120	84
10	3.9	200	224	22	710	29
13	4.0	142	167	34	960	37
80[2]	4.1	[2]20	[2]36	95	1,320	79
Av	4.1±0.2	157±78	180±31	47±29	1,380±500	66±30
83[2]	6.1	25	37	[3]~176	1,970	151

Av Arithmetic average and standard deviation.
NA Not available.
[1]Belt fire growth rate from time of belt ignition until start of belt flame spread. Calculated by $\alpha_{SBR} = (Q_{BFS} - Q_{BI})/(t_{BFS} - t_{BI})$.
[2]Data are from tables 4 and 5 of reference 3 and are not included in "average" values of t_{BI} and t_{BFS}.
[3]Data calculated using equations 7 and 8 of reference 3 at time equal to 24.6 min.

Table 4.—Experimental heat release rates (Q_{BI} and Q_{BFS}), normalized by local velocity, and calculated and experimental fire growth rates (α_{SBR}) for SBR belting

V_0, m/s	Q_{BI}/V_0, kJ/m	Q_{BFS}/V_0, kJ/m	α_{SBR}, kW/min	
			Calculated[1]	Experimental
0.76	37	490	7	7±5
1.6	30	340	20	20±7
4.1	11	340	82	66±30
6.1[2]	[2]29	[2]320	150	[2]143
Av	27±11	394±180	NAp	NAp

Av Arithmetic average and standard deviation.
NAp Not applicable.
[1]Fire growth size calculated from equation 2, $\alpha_{SBR} = 9.9\ V_0^{1.5}$.
[2]Based on earlier fire test (reference 3).

Table 5.—Predicted and measured fire growth elapsed times (Δt_{PRED} and Δt_{EXPTL}) from belt ignition until belt flame spread

V_0, m/s	Δt_{PRED},[1] min	Δt_{EXPTL}, min
0.76	43	58
1.6	29	42
4.1	18	23

[1]Calculated from equation 6, $\Delta t_{PRED} = 37.1\ V_0^{-0.5}$.

The total time available to control and extinguish the belt fire (t_{EXTING}) can be estimated by adding the predicted elapsed time from belt ignition until belt flame spread (equation 6) to the average alarm times of detection relative to the time of belt ignition (column 5 or 6, table 2). The time between fire detection and belt flame spread is an estimate of the time that could be used to control and extinguish the localized belt fire before the spread of the flames. Once flame spread begins, the ability to control and extinguish the fire significantly diminishes. On the average, the predicted times are lower than the measured times and provide some margin of safety for estimating the time available for fire extinguishment. The estimated t_{EXTING} using CO sensors is about 73 min at the 0.76-m/s airflow and about 46 min at 4.1-m/s airflow. The use of smoke sensors instead of CO sensors would increase the respective t_{EXTING} times to 90 min and 52 min.

PRODUCTION OF CO AND SMOKE

During the early stages of belt burning, appreciable levels of CO and smoke are released. As has been found in a previous study (*3*), the level of CO in parts per million and the optical density of smoke in inverse meters are linearly related to the heat release rate (Q_{SBR}) and inversely related to the local ventilation airflow via the following expressions:

$$CO_{ppm} = \frac{B_{CO}\ Q_{SBR}}{V_0\ A_0}, \qquad (7)$$

and

$$D_{m^{-1}} = \frac{B_D\ Q_{SBR}}{V_0\ A_0}, \qquad (8)$$

where B_{CO} = the production constant of CO, $ppm \cdot m^3/kJ$,

B_D = production constant of smoke, $m^{-1} \cdot m^3/kJ$,

and A_0 = tunnel cross-sectional area.

CO Production

The B_{CO} (average) values and the maximum CO concentrations from these experiments are given in table 6 at the two belt-to-roof separation distances and at the various airflows, assuming that V_0 is approximately equal to V_e. The V_0 value varied during the belt burning, and its instantaneous local value is not known, whereas the exit velocity was monitored during the test. The B_{CO} (average) values in column 4 were determined during belt flame spread until the peak heat release rate occurred. During this time, the CO was produced almost exclusively by the conveyor belt since the wood roof was not involved until belt flames reached the end of the belt sample. The CO_{MAX} values in column 5 are 1-min averaged maximum levels of CO obtained in each test.

The data of table 6 indicate that the overall average B_{CO} value for the fire-resistant SBR belting is 5.5 ± 3.0, in excellent agreement with the 5.7 value previously reported (*3*). However, the average values of B_{CO} at each average velocity decreased as the air velocity increased (see equation C-15 in appendix C). The B_{CO} also varied with the belt-to-roof distance (see table 6). A comparison of the maximum levels of CO (column 5 of table 6) shows an average value of 1,430 ppm at the low airflow and a value of 750 ppm at the high airflow for the 1.4-m belt-to-roof distance. The greatest CO concentration measured was 4,090 ppm for test 14 at the 0.8-m belt-to-roof distance and at an airflow of 0.62 m/s. These measured CO values are based on burning a 12.8-m-long belt and, in some tests, the wood roof. Larger values can occur, especially for fuel-rich fires (see appendix C).

Smoke Production

During these experiments, no data were obtained for the optical density of the smoke produced. However, considering the excellent agreement of the present data with the B_{CO} values reported in reference 3, one expects the smoke-to-CO ratio to be approximately the same as that given in reference 3 during the early stage of belt burning. From reference 3 data, the production parameter for

smoke optical density (B_D) and the production parameter for CO (B_{CO}) had a ratio of

$$\frac{B_D}{B_{CO}} = 0.011. \quad (9)$$

Assuming that this ratio remains constant, then the production parameter for smoke optical density would also be independent of air velocity. The critical level for visibility below which the probability of escape is marginal is about 3.7 m (*5-6*). The visibility, in meters, and optical density are related by

$$VIS(m) = \frac{0.8}{D}. \quad (10)$$

Then, the critical level of optical density (D_{CRIT}) becomes

$$D_{CRIT} \geq \frac{0.8}{3.7} = 0.22\ m^{-1}. \quad (11)$$

With this information, the heat release rates at this critical level of optical density (Q_{CRIT}) may be estimated at any flow using equation 8. At the time of belt ignition, the average heat release rate normalized by airflow (table 4, column 2) is 27 kJ/m; the value of B_D can be calculated from equation 9 using an average B_{CO} value for SBR belting. Equation 8 for airflows from 0.76 to 6.1 m/s becomes at the time of belt ignition

$$Q_{CRIT} = \frac{D_{CRIT} V_0 A_0}{B_D}. \quad (12)$$

The smoke production constants, critical heat release rates (Q_{CRIT}), CO concentrations, and elapsed times from belt ignition until the occurrence of the critical optical density are given at 0.76-, 1.6-, and 4.1-m/s airflows in table 7. For all velocities, the critical level of optical density is reached approximately when the belt ignites and is exceeded very rapidly after ignition of the belt. The level of CO is about 15 to 19 ppm at the time of critical optical density and is approximately independent of airflow. By the time the belt heat release rate has reached the level necessary for belt flame spread (394 kJ/m, column 3 of table 4), the estimated visibility using equations 8 and 10 is less than 0.3 m.

The relationships between production constants B_{CO} and B_D and yields of CO (Y_{CO}) and smoke (Y_S), respectively, are discussed in appendix D. These experimental CO and smoke yields are directly related by a constant factor, 2.1, whereas the literature value for several combustible solids is 2.3±0.4 (*7*).

Table 6.—CO production constants (B_{CO}) from burning SBR belting and maximum CO at two belt-to-roof separations (H_{BR}) and various tunnel airflows (V_c)

Test	H_{BR}, m	V_c, m/s	$B_{CO}(av)$, ppm•m³/kJ	CO_{MAX}, ppm
		LOW AIRFLOW		
3	1.4	0.68	6.1±1.1	600
4	1.4	0.73	6.4±2.1	1,240
12	1.4	0.74	4.3±1.0	2,440
Av ...	1.4	0.72±0.03	5.6±1.1	1,430±900
14	0.8	0.62	7.6±2.7	4,090
16	0.8	0.64	13.3±6.6	2,810
Av ...	0.8	0.63±0.01	10.5±4.0	3,450±900
		MEDIUM AIRFLOW		
7	1.4	1.4	4.1±1.0	1,520
15	0.8	1.2	7.3±2.0	2,590
		HIGH AIRFLOW		
2	1.4	2.8	2.9±0.4	630
5	1.4	3.1	3.7±0.2	650
6	1.4	3.7	4.1±0.5	640
10	1.4	3.4	3.1±0.4	1,090
Av ...	1.4	3.3±0.4	4.0±0.6	750±200
13	0.8	2.7	2.7±0.7	1,320
Overall av ..		NAp	5.5±3.0	NAp

Av Arithmetic average and standard deviation.
NAp Not applicable.

Table 7.—Smoke production constants (B_D), critical heat release rates (Q_{CRIT}), CO concentrations, and elapsed times from belt ignition until critical optical density of 0.22 m^{-1}

V_0, m/s	B_D, m^{-1}•m^3/kJ	Q_{CRIT}, kW	CO, ppm	$t_{CRIT} - t_{BI}$, min
0.76	0.060	21	15	<0.0
1.6	0.054	47	19	0.18
4.1	0.038	175	19	1.60

BELT AND ROOF FLAME PROPAGATION AND BELT-TO-ROOF SEPARATION EFFECTS

The data presented and analyzed thus far were gathered primarily during the initial stages of fire growth prior to the onset of belt flame spread, when the belt-to-roof separation effects are minimal. Only those tests in which the coal fire ignited the belt, resulting in belt flame propagation, will be considered here. Three tests of sixteen did not spread belt flames, two tests (tests 8 and 9) at 0.76 m/s airflow and one test (test 11) at 4.1 m/s airflow. For these tests, the coal pile flames diminished after three of the six electrical heaters failed at about 162 to 170 min.

The subsequent stage of belt flame spread increases the hazard level dramatically because of the greater heat release and fire growth rates. The belt-to-roof separation

distance, which affects these rates, is examined in the following paragraphs.

Tests 1 through 12 were conducted with a top belt-to-roof separation of 1.4 m, and tests 13 through 16 were conducted at a belt-to-roof separation of 0.8 m. As should be expected, the ignition of the wood roof by the burning belt was more difficult at the larger separation and at the highest airflows.

At the 1.4-m belt-to-roof separation and the highest air velocity (4.1 m/s), only test 10 resulted in a propagating roof flame spread. The flames started at about the 10th roof plank from the front, charred the next six planks, and destroyed the last nine roof planks. In test 2, roof flames lightly charred the last 13 roof planks; in test 5, flames flashed over the surface and slightly charred the last several roof planks. In test 6, only scorching and soot were observed on the last 11 roof planks.

At both the intermediate airflow and the lowest airflow, all five tests, 1, 3, 4, 7, and 12, resulted in total roof destruction. In test 7, at an airflow of 1.4 m/s, the wood roof flames flashed over 6 m of roof about 4 min after the belt flame spread began. The roof flames self-extinguished but after several minutes reignited; meanwhile, the belt flames had propagated to the end of the belt. The roof reignited at its downstream end, with flames that propagated against the airflow at a rate of 0.4 cm/s, destroying the roof.

All four tests, 13, 14, 15, and 16, at the 0.8-m belt-to-roof separation resulted in roof flame spreads and complete destruction of the roof planks. Tests 14 and 16 were at the 0.76-m/s airflow; tests 13 and 15 were at the 4.1- and 1.6-m/s airflows, respectively.

One-minute average values of the maximum CO concentrations and maximum heat release rates, average belt and roof flame spreads, and average fire growth rates during flame spread for all the tests except test 7 (see above discussion) are summarized in table 8 at 0.76-, 1.6-, and 4.1-m/s airflows and two belt-to-roof separations. The heat release rates were calculated from the CO and CO_2 concentrations using equation B-2 in appendix B. The rates for both belt and roof flame spread for each test are given in appendix C, table C-2. The smaller belt-to-roof separation (H_{BR} = 0.8 m) resulted in (1) higher levels of CO, (2) larger heat release rates, (3) more rapid flame spread rates, both along the belt surface and along the roof, and (4) more rapid fire growth rates.

For the three tests at the highest airflow for which there were no sustained roof flames (tests 2, 5, and 6), all of the fire hazard averaged values were lower (e.g., maximum CO = 640 ppm (table 6), Q_{MAX} = 4,800 kW (table C-3), belt flame spread = 0.75 cm/s (table C-2), and α_{FS} = 280 kW/min) than the corresponding values for tests at the 4.1-m/s airflow that resulted in sustained roof flame spread.

As the distance from the belt to the roof decreases, the resultant heat flux at the roof from the belt flame increases roughly inversely as the square of the distance. The increased heat flux results in a more rapid ignition of the roof surface. Also, once both belt and roof are burning, there is a more rapid rate of fuel generation and consumption, resulting in higher heat release rates, larger CO levels, and faster flame spread rates. It is likely that the chosen belt-to-roof separation of 0.8 m is not optimum for maximizing either flame spread rates or heat release rates. Closer separation distances will not necessarily increase fire hazards since the heating and the spread rate of the burning fuel will eventually be limited by the decreased oxygen. In the data reported in this section and displayed in table 8, however, it can be seen that a burning conveyor belt represents a more hazardous condition at the 0.8-m belt-to-roof separation than at the 1.4-m separation.

Table 8.—Maximum average CO concentrations (CO_{MAX}) and heat released (Q_{MAX}), average belt and roof flame spreads, and fire growth rates (α_{FS})

V_0, m/s	H_{BR}, m	CO_{MAX},[1] ppm	Q_{MAX},[1] kW	Av flame spread rate, cm/s		α_{FS},[2] kW/min
				Belt	Roof	
0.76	1.4	1,400	2,100	0.66	0.96	37
	0.8	3,500	6,100	12.5	10.4	870
1.6	1.4	1,500	2,800	1.0	3.6	210
	0.8	2,600	6,200	2.0	4.1	510
4.1	1.4	750	5,800	0.86	1.0	410
	0.8	1,300	15,000	2.0	6.1	1,700

[1]1-min average maximum.

[2]Fire growth rate during belt flame spread (see also appendix table C-4).

TEMPERATURE HAZARD

As discussed in earlier sections, the levels of CO and smoke vary proportionally to the ratio (Q/V_0A_0) times some constant (i.e., B_{CO} for CO, or B_D for smoke, in equations 7 and 8, respectively). Similarly, there is a net flow of heat from the fire, which can also be related to the fire size. Hwang (*8*) found that the average increase in air temperature downstream of a fire can be related to the heat release rate (Q) in kilowatts via

$$\Delta T_{AV}(\ell) \equiv (T_{AV}(\ell) - T_0) = \frac{Q}{\rho_0 C_0 V_0 A_0} \times e^{-\gamma \times \ell}, \quad (13)$$

where T_0 = initial or ambient temperature, about 18.3 °C,

ρ_0 = air density at T_0, 1.2 kg/m^3,

C_0 = heat capacity of air at T_0, 1.088 J/g•K,

γ = convective heat transfer parameter,

and ℓ = distance downstream of the fire.

The tunnel or gallery airflow is assumed to be uniform, so the local velocity is equal to the average tunnel velocity. The parameter γ depends on the heat transfer coefficient h and can be expressed as (*8*)

$$\gamma = \frac{h\, P_0}{\rho_0 C_0 V_0 A_0}, \quad (14)$$

where A_0 = entry cross-sectional area, 7.53 m^2

and P_0 = entry perimeter, 11.5 m.

A reasonable value of h for fully established turbulent flow is given by

$$h = 7.4\times10^{-3} \times \frac{V_0^{0.8}}{d_H^{0.2}}, \quad (15)$$

where d_H is the hydraulic diameter of the given entry, defined by

$$d_H = \frac{4\, A_0}{P_0}. \quad (16)$$

Equation 14 therefore becomes

$$\gamma(P_0, A_0, V_0) = 4.3\times10^{-3} \left[\frac{P_0}{A_0}\right]^{1.2} V_0^{-0.20}, \quad (17)$$

which for this tunnel entry becomes

$$\gamma(V_0) = 7.2\times10^{-3} V_0^{-0.20}. \quad (18)$$

Substituting equation 17 (or equation 18) into equation 13 gives

$$\Delta T_{AV}(\ell, V_0, A_0) = 0.77\, e^{\left(-\ell \times 0.0043 \left[\frac{P_0}{A_0}\right]^{1.2} V_0^{-0.20}\right)} \left[\frac{Q}{V_0 A_0}\right]$$

$$= 0.77\, e^{(-\ell \times 0.0072 V_0^{-0.20})} \left[\frac{Q}{V_0 A_0}\right], \quad (19)$$

which expresses the temperature rise in this entry at some distance downstream of the fire for a given velocity and heat release rate (kilowatts).

Consequently, an air temperature hazard parameter can be written as

$$B_T = 0.77\, e^{-\ell \times 0.0043 \left[\frac{P_0}{A_0}\right]^{1.2} V_0^{-0.2}}, \quad (20)$$

where the value of B_T depends upon the distance from the fire, entry perimeter length divided by area, wall roughness, and air velocity. The B_T parameter is sensitive to air velocity, wall temperatures, and wall roughness because heat losses vary directly with the temperature difference between the gases and the entry walls, both through radiation and convection transfer.

The maximum internal body temperature that a human can tolerate without medical consequences is generally accepted to be approximately 40 °C. Exposure to an ambient temperature of 40 °C will rapidly raise the normal body temperature (37.0 °C) to the hazardous level in an interval as short as 60 min for unacclimatized resting individuals in a water-saturated environment (*9*). Higher ambient temperatures and increased physical activity such as may occur during escape will shorten the survival time period.

The length of time at a fixed location and air velocity that the entry is less than 40 °C during a fire can be calculated from equation 9 using the estimated heat release rate divided by the experimental fire growth rate α_{FS} (column 3 of table 9). A typical mine entry has an ambient temperature of approximately 18 °C. The calculated heat release rates (Q) to achieve the 22 °C temperature rise to 40 °C at three air velocities based on these tunnel parameters at ℓ = 305 and 610 m are given in columns 4 and 6 of table 9, respectively. The times to increase entry temperatures are calculated by dividing the respective calculated Q values (columns 4 or 6 in table 9) by the experimental α_{FS} values (column 3 of table 9). The resulting

Table 9.—Fire growth rates (α_{FS}), heat release rates (Q), and times (Δt) to achieve 40 °C at 305 and 610 m from fire

V_0, m/s	H_{BR}, m	α_{FS}, kW/min	ℓ = 305 m		ℓ = 610 m	
			Q,[1] MW	Δt,[2] min	Q,[1] MW	Δt,[2] min
0.76	1.4	37	1.57	43	16.8	460
	0.8	870	1.57	2	16.8	19
1.6	1.4	210	2.24	11	18.0	87
	0.8	510	2.24	4	18.0	35
4.1	1.4	410	3.93	10	19.6	48
	0.8	1,700	3.93	2	19.6	13

[1]Q is the calculated heat release rate at fire source to achieve 40 °C at specified distance ℓ.

[2]$\Delta t = t_{CRIT} - t_{BFS}$, where t_{CRIT} is time at which temperature is 40 °C at specified distance ℓ and t_{BFS} is time of initial belt flame spread.

times are given in columns 5 and 7 in table 9, respectively, for the three different air velocities and the two belt-to-roof separation distances, 1.4 and 0.8 m.

The effect of a lower fire growth rate (see α_{FS} for H_{BR} = 1.4 m compared with H_{BR} = 0.8 m, at 0.76- and 4.1-m/s air velocities) is clearly evident, and the lower rate results in longer times to achieve 40 °C. However, even for the lower heat release rates at the larger belt-to-roof distance, the temperatures at some distance downstream of the fire would still be intolerable. The calculated air temperature (equation 19) is still above 40 °C for ℓ equal to 290 to 460 m. For distances of 90 to 200 m downstream, the calculated air temperature is above 100 °C at the lower heat release rates.

Figure 3 shows 40 °C isotemperature lines calculated using equation 19 for positions at 300, 400, 500, and 600 m downstream from the fire source as a function of heat release rate and air velocity. The area above any constant position curve (e.g., ℓ = 600 m) represents points that would have downstream air temperatures greater than 40 °C along the increasing Y-coordinate for the same airflow, or along the decreasing X-coordinate for the same fire size. For example, the experimental point shown at 4.1 m/s, 14,500 kW would result in temperatures above 40 °C at the 500-m position, but temperatures would be less than 40 °C at the 600-m position unless the airflow were reduced to about 0.76 m/s.

Experimental averaged values from table 8 are shown in figure 3 for the belt-to-roof separations at 0.8 and 1.4 m. Two experimental values at 1.0- and 4.1-m/s airflows are included from recent work[7] in which two 15-m strands of R11 (SBR) conveyor belting were burned, with the top belt 1.3 m from a noncombustible roof. All of these fire experiments indicate hazardous-to-life temperatures up to a distance of 305 m from the fire source. For the maximum heat release values, these hazardous temperatures can extend even up to distances as far as 500 m.

Downstream roof gas temperatures at 27.4 m (tunnel exit) ranged from 650 °C at the 0.76-m/s airflow for the belt-to-roof separation of 0.8 m to a low temperature of 250 °C at the 4.1-m/s airflow for the belt-to-roof separation of 1.4 m. The roof gas temperatures are summarized in appendix table E. At the two lower airflows, significant rollback of combustion products occurred, as evident by high temperatures of upstream roof gas. Upstream roof gas temperatures at the 0.0-m tunnel distance (2.7 m upwind of the coal pile) ranged from 800 °C at the

Figure 3

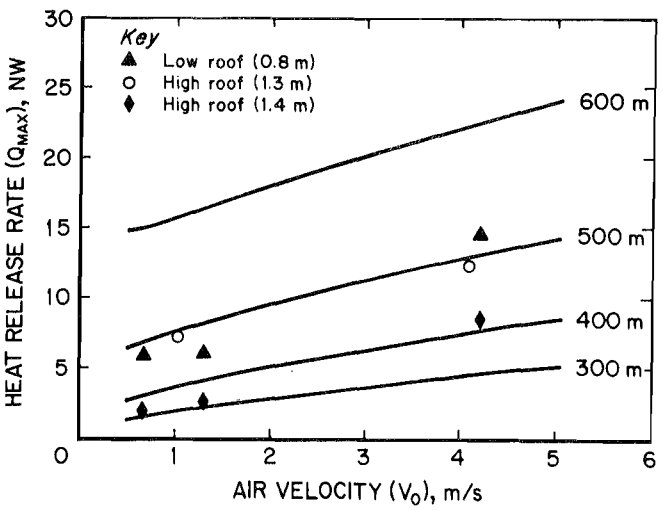

Calculated 40 °C isotemperature lines at different heat release rates and air velocities. Maximum experimental heat release rates are shown for three belt-to-roof separations.

[7]Private communication. Mark Ryan, Fires, Explosions, and Explosives Group, Pittsburgh Research Center, U.S. Bureau of Mines.

0.76-m/s airflow for the belt-to-roof separation distance of 0.8 m to a low temperature of 20 °C at the 4.1-m/s airflow for the belt-to-roof separation distance of 1.4 m.

CO PEAK VALUES AND TOXIC HAZARDS

Clearly, heat is one of the major life threats in conveyor belt fires with growth rates at the magnitudes observed in these tests. However, CO is also a significant life threat because of its insidious narcotic behavior in cumulative doses.

The average maximum levels of CO measured in these experiments were presented in a previous section (column 3 of table 8). While the absolute level of CO is important (1%, or 10,000 ppm, is considered lethal in less than 10 min), cumulative exposure to lower levels of CO over longer time periods can also be lethal.

The toxic CO load from burning conveyor belts, wood, or coal can be the major agent causing human incapacitation, thus preventing escape. Exposed, unprotected persons poisoned by CO often pass through a narcotic sleep stage in which they have neither the desire nor the motivation to escape. They soon become physically unable to escape and rapidly expire. The time (t_{INCAP}) available for unaided escape can be calculated from the concentration of CO in the breathing air and the potential exposure time (*10*). The toxic CO load, based on animal studies, is about 36,500 ppm•min, with a threshold value (no discernible toxic effect) of about 233 ppm. For example, the incapacitation toxic load for a 30-min exposure of 138 rats to a steady CO concentration of 1,778 ppm gives an experimental value for the toxic load of 43,500 ppm•min (*11*). This same nominal level of toxic load is incapacitating for the class of mammals (rats, baboons, or humans) apparently because of the narcotic effect of anemic hypoxia, which interferes with their escape skills through a common mechanism.

The physical activity of the victim and the presence of other toxic agents and deleterious conditions (low oxygen levels, high CO_2 levels, smoke, heat) determine the actual time to incapacitation at a fixed concentration of CO. The value 36,500 ppm•min is for incapacitation of an unprotected person at rest.

The threshold CO level of 233 ppm was used as the safe lower limit for calculating the time available for an escape. The experimental CO maximum values, the time to the CO maximum from the start of heating the coal pile, and the shortest time in which an incapacitation dose of CO occurred are shown in columns 3, 4, and 5 of table 10, respectively, for all the experiments in which the belt and wood roof propagated flames. The t_{INCAP} value is the experimental time from the start of heating the coal pile until the time-integrated concentration (adjusted with respect to the threshold value) equals the toxic incapacitation dose rate, or toxic load for CO, of 36,500 ppm•min. The t_{INCAP} values can be calculated from the summation of the time-dependent CO levels as follows:

$$\sum_{t_i = 0}^{t_i = t_{INCAP}} [C(t_i) - 233]\,\delta t_i = 36{,}500 \text{ ppm•min}, \quad (21)$$

where the experimental concentration C(t) varies with time and only bracket [...] values greater than zero are summed. The δt period is the elapsed time between sample points and was 0.0833 min (5 s). Any exposure time longer than t_{INCAP} would result in collapse of unprotected persons downwind of the fire.

The time during which the CO concentration rises from 233 ppm until an incapacitation dose occurs is defined here as the experimentally determined critical time (t_{CRIT}) and is given in column 6 of table 10. This time is the worst case under these limited fuel conditions.

Greater CO levels are possible during flame spread for larger fuel loadings. These theoretical CO levels and t_{CRIT} values are given in columns 7 and 8 of table 10, respectively. The theoretical values were derived assuming steady-state flame spread along a single strand of SBR belting. The value was then doubled to account for the two strands of belting used in conveyor systems.

The average t_{INCAP} is 240±25 min and includes about 160 min of coal smoldering and flaming, which gave an alarm at about the 10-ppm CO level in 131±20 min (see appendix E table). There were no statistically significant effects of airflow over the range of 0.75 to 4.5 m/s during this early stage of fire development.

The experimentally determined elapsed time (column 6 of table 10) t_{CRIT} during rapid belt fire growth from 233 ppm until t_{INCAP} averaged 42±14 min, with no statistically significant effect of airflow at the 95% confidence level. Table 11 shows the average experimentally determined t_{CRIT} values of table 10 for the three average airflow groups and two belt-to-roof distances. The belt-to-roof distance effect is significant at the 95% confidence level, whereas the effect of airflow is not.

Assuming CO levels remained constant, successful rescue of unprotected miners must occur within about three to four times the t_{CRIT} time period.

Table 10.—Experimental and theoretical CO maximum values, times to maximum concentrations, and experimental and theoretical times to incapacitation (t_{CRIT})

Test	V_e, m/s	Experimental				Theoretical	
		CO_{MAX}, ppm	Time to CO_{MAX}, min	t_{INCAP},[1] min	t_{CRIT},[2] min	CO,[3] ppm	t_{CRIT},[4] min
			LOW AIRFLOW				
4	0.73	1,240	233	256	49	4,500	8.2
12	0.74	2,440	202	229	45	4,500	8.1
14	0.62	4,090	263	279	27	4,000	9.1
16	0.64	2,810	212	228	23	4,100	8.9
			MEDIUM AIRFLOW				
7	1.4	1,520	200	219	34	6,300	5.8
15	1.2	2,590	244	256	22	5,900	6.2
			HIGH AIRFLOW				
2	2.8	630	168	203	56	6,600	5.5
5	3.1	650	207	256	57	6,400	5.7
6	3.7	640	173	232	60	5,800	6.3
10	3.4	1,090	235	269	43	6,100	6.0
13	2.7	1,320	177	211	43	6,700	5.5

[1]Experimental time for incapacitation dose calculated from start of heating until integrated CO level (36,500 ppm•min) of adsorbed toxic would cause incapacitation of an unprotected person at rest.

[2]Time increment during rapid fire growth from time when CO is 233 ppm until integrated dose would cause incapacitation at t_{INCAP}.

[3]Theoretical CO concentrations calculated from appendix C, equation C-16, assuming air-limited belt burning.

[4]Theoretical critical times for incapacitation calculated by dividing incapacitating dose, 36,500 ppm•min, by air-limited belt-burning CO concentration (column 7).

Table 11.—Time elapsed, in minutes, from 233 ppm CO until occurrence of incapacitation

V_e, m/s	H_{BR} = 1.4 m	H_{BR} = 0.8 m
0.68	47±2	25±3
1.3	34	22
3.1	54±8	43

FIRE HAZARD PARAMETER

Inspection of equations 7, 8, and 19 reveals that the hazards of CO, smoke, and excessive temperature downstream of the fire can be scaled with the ratio of heat release rate to ventilation airflow rate $[Q_{FIRE}/(V_0A_0)]$. This ratio is defined as the fire hazard parameter (FHP) and represents a measure of the relative hazards. As the heat release rate increases for a fixed airflow, the levels of CO, smoke, and temperature increase directly. For a fixed heat release rate, these levels increase as the airflow decreases. Based upon the data obtained from this series of tests, the production constant for CO varied with the ventilation airflow according to appendix equation C-15. This means that the level of CO is a function of the FHP and the airflow. For smoke, it is assumed that a constant ratio of the smoke optical density to CO concentration is valid without any dependence on air velocity.

For downstream air temperatures, the production constant for temperature at any distance ℓ was found to be affected by air velocity according to equation 20. Figure 4 is a representation of the magnitude of the FHP necessary

Figure 4

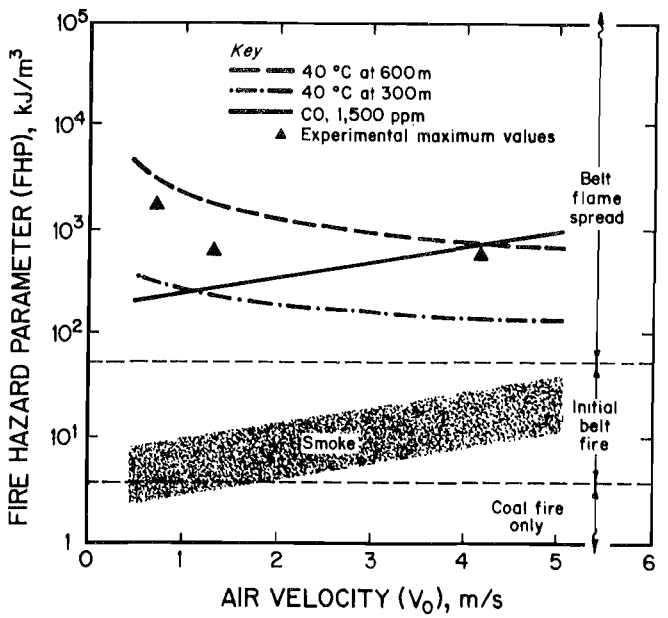

Critical values of smoke, CO, and temperature at various fire hazard parameter values. The fire growth stages of coal fire only, initial belt fire, and belt flame spread are superimposed.

to produce critical levels of CO and smoke at any point downstream of the fire, and critical levels of temperature at 300 and 600 m downstream of the fire for this gallery with a cross-sectional area of 7.53 m^2. The FHP necessary to result in a CO concentration of 1,500 ppm increases as the air velocity increases, rising from a value of 215 at 0.76 m/s to a value of 950 at 5 m/s.

The shaded "smoke" area in figure 4 delineates the range of smoke obscuration with about a 4-m visibility at its lowest edge to the critical 1-m visibility at its upper edge. The 4-m visibility starts at an FHP value of about 2 at 0.5 m/s airflow and increases to an FHP value of 10 at 5 m/s airflow. The upper edge of the smoke area, representing a critical visibility of 1 m, also increases with airflow. The smoke area coincides with the initial belt fire stage and begins approximately after the "coal fire only" stage is completed. Experimental maximum values of the FHP are also shown at three airflows.

The data of figure 4 indicate that critical values of the FHP for smoke, CO, and temperature are exceeded at all distances less than 300 m downstream of the fire. Figure 4 also indicates that critical values of the FHP are obtained only during the stage of belt flame spread for CO and temperature, while for smoke, critical values of the FHP occur during the early stage of belt burning.

The life-threatening hazards of smoke obscuration and CO toxicity decreased as the airflow increased because dilution, provided by the ventilation, more than compensated for the increased fire growth rate under these test conditions. However, fire growth rates, both during the early stages of belt burning and during the stage of flame spread, increased with air velocity.

CONCLUSIONS

Fires that develop within conveyor belt entries can present significant hazards to underground personnel. The major hazards studied in this report were reductions in visibility due to smoke, elevated levels of CO that can result in incapacitation, and elevated temperatures that can produce intolerable levels of heat stress. Severe reductions in visibility resulted very quickly once the belt ignited. High CO and temperature levels were found to occur during the stages of flame spread along the surface of the conveyor belt and the wood roof.

All of these hazards were found to scale with the ratio of heat release rate to ventilation airflow. The scaling parameters (called production constants) were also found to depend upon the ventilation air velocity. The ratio of heat release rate to volumetric ventilation airflow rate is termed the "fire hazard parameter" (FHP), not only because the hazards scale with this quantity, but also because the points of transition from one stage of fire development to the next scale with the same FHP parameter.

As the initial coal fire grows, it eventually ignites the belt. At the time of belt ignition, the FHP is 3.6, and it increases to a value of 52 when sustained belt flame spread occurs.

The elapsed times between the transitions from one stage of fire development to the next depend upon the rates of fire growth within each stage. During the coal fire stage, the growth rates are slow, the net result being that the time from onset of flaming coal to the time of belt ignition increases as the air velocity increases. During the early stage of belt burning, the fire growth rates increase dramatically and there is a strong dependence of the fire growth rate on the air velocity, the result being that the time from belt ignition to the onset of belt flame spread decreases as the air velocity increases. During the stage of flame spread, the rates of fire growth increase again, accelerating the onset of critical levels of CO and heat downstream of the fire.

At low air velocities, the fires tend to grow more slowly, but there is less dilution of contaminants. As the air velocity increases, the fires tend to grow more rapidly, but there is much greater dilution of contaminants. The end result is that the time to incapacitation by CO, as measured from the time of belt ignition, remains relatively constant, independent of the air velocity. For all the tests that resulted in flame spread, the time from belt ignition to incapacitation by CO averaged 85 min.

Estimates of the time from belt ignition to the time at which the heat release rate is sufficient to produce a temperature in excess of 40 °C at 305 m downstream of the fire averaged 36 min, and the time decreased with air velocity from a value of 53 min at 0.76 m/s to a value of 22 min at 3.2 m/s.

Estimates of the times to reach critical levels of visibility because of smoke obscuration indicated that these times tend to coincide closely with the time of belt ignition. Although the toxicological aspects of elevated levels of smoke are not well known, reduced visibility can significantly impact the evacuation of personnel.

The data also reveal that the proximity of the roof to the surface of the conveyor belt plays a major role not only with regard to flame spread rates but also with regard to the potential of the belt fire to spread to the roof and the level of hazard that results. Data acquired at a belt-to-roof distance of 0.8 m indicated more rapid flame spread rates, greater heat release rates, and increased levels of CO than data obtained at a belt-to-roof distance of 1.4 m.

Clearly, the transition of these fires from one stage to the next represents increasing levels of hazard. The question naturally arises as to methods available to reduce or eliminate the probability that personnel will be exposed to these hazards. Conveyor belts with improved flame-resistant properties have been shown to significantly reduce the potential for flame spread, thereby reducing the probability of exposure to the life-threatening hazards of

CO and heat, which were shown to occur during the stages of flame spread.

Early-warning fire detection systems also have a strong impact on the probability of miners' exposure to these fire hazards. Application of previously developed criteria in reference 3 for the use of CO and smoke sensors for early-warning fire detectors in conveyor entries indicated that smoke sensors provided an average warning of 40 min before belt ignition and CO sensors an average warning of 28 min before belt ignition. Clearly, the efficient utilization of these times for evacuation and control of the developing fire is essential in order to ensure the safety of the mine personnel, but the fact that sensors provided this early-warning capability is just as significant. It was also found that point-type heat sensors would provide no early warning capability, but would alarm on the average 34 min after the belt ignited.

ACKNOWLEDGMENTS

The authors would like to thank Robert Scaramozzino and Thomas Rabbitt, representatives of the United Mine Workers of America, for their helpful discussions at the planning stage and during these tests. Recognition is due William C. Beasley, mechanical engineer, Mark E. Schwartz, electrical engineer technician, and Harry C. Verakis, supervisory general engineer, of the Approval and Certification Center of the Mine Safety and Health Administration, U.S. Department of Labor, Triadelphia, WV, for their assistance during the experiments.

REFERENCES

1. Fidago, C. J. Summary of Underground Coal Mine Fires 1980 Through 1992. Ind. Saf. Div., Mine Safety and Health Admin., Pittsburgh, PA., Rep. 02-098-93, Apr. 9, 1993, 12 pp.

2. Roberts, A. F. Review Paper: Mine Fires. Paper in Proceedings of the 23rd International Conference of Safety in Mines Research Institutes (Washington, DC, Sept. 11-15, 1989). USBM OFR 27-89, 1989, pp. 3-21; NTIS: PB89-225262/AS.

3. Litton, C. D., C. P. Lazzara, and F. J. Perzak. Fire Detection for Conveyor Belt Entries. USBM RI 9380, 1991, 23 pp.

4. U.S. Code of Federal Regulations. Title 30—Mineral Resources; Chapter I—Mine Safety and Health Administration, Department of Labor; Subchapter B—Testing, Evaluation, and Approval of Mining Products; Part 18—Electrical Motor Driven Mine Equipment and Accessories; Subpart C—Inspections and Tests; Section 18.65—Flame Test of Conveyor Belting and Hose; 1994.

5. Jin, T. Visibility Through Fire Smoke. J. Fire Flammability, v. 9, 1978, pp. 135-155.

6. Kissel, F. N., and C. D. Litton. How Smoke Hinders Escape From Coal Mine Fires. Min. Eng. (N.Y.), v. 44, No. 1, Jan. 1992, pp. 79-83.

7. Mulholland, G. W., S. Yusa, M. Janssens, W. Twilley, and V. Babrauskas. Effect of Oxygen Concentration on CO and Smoke Produced by Flames. Paper in Proceedings of International Symposium on Fire Safety Science (3rd), Edinburgh, Scotland, July 8-12, 1991. Elsevier Sci. Publ. Ltd., 1991, pp. 585-594.

8. Hwang, C. C., and R. F. Chaiken. Effect of Duct Fire on the Ventilation Air Velocity. USBM RI 8311, 1978, 19 pp.

9. Bell, C. R. Heat and Hot Work. Sec. in Encyclopedia of Occupational Health and Safety, ed. by L. Parmeggiani. Int. Labour Organ., Geneva, 3rd ed., 1983, v. 1, pp. 1018-1020.

10. Kaplan, H. L., A. F. Grand, W. R. Rogers, W. G. Switzer, and G. E. Hartzell. A Research Study of the Assessment of Escape Impairment by Irritant Gases in Postcrash Aircraft Fires. Southwest Res. Inst., San Antonio, TX, Final Rep. DOT/FAA/CT-84/16, Sept. 1984, 65 pp.

11. Hartzell, G. E., D. N. Priest, and W. G. Switzer. Mathematical Modeling of Toxicological Effects of Fire Gases. Paper in Fire Safety Science—Proceedings of the First International Symposium. Hemisphere Publ. Corp., 1986, pp. 1059-1068.

12. Tewarson, A. Heat Release Rate in Fires. Fire Mater., v. 4, No. 4, 1980, pp. 185-191.

13. Parker, W. J. Calculations of the Heat Release Rate by Oxygen Consumption for Various Applications. Nat. Bur. Stand. Rep. NBSIR 81-2427-1, 1982, 41 pp.

14. Dobbins, R. A., G. W. Mulholland, and N. P. Bryner. Comparison of a Fractal Smoke Optics Model With Light Extinction Measurements. Atmos. Environ., v. 28, No. 5, Mar. 1994, pp. 889-897.

15. Tewarson, A. Generation of Heat and Chemical Compounds in Fires. Ch. in The SFPE Handbook of Fire Protection Engineering, ed. by P. E. DiNenno. Natl. Fire Prot. Assoc., 1st ed., 1988, pp. 1-179 to 1-999.

APPENDIX A.—LIST OF SYMBOLS AND ABBREVIATIONS

Symbols

A_0	entry cross-sectional area (7.53 m^2 for this fire gallery), m^2
B_{CO}	CO production constant, $ppm \cdot m^3/kJ$
B_D	smoke production constant, $m^{-1} \cdot m^3/kJ$
B_T	air temperature hazard parameter, $°C \cdot m^4/kJ$
BFS	subscript denoting belt flame spread
BI	subscript denoting belt ignition
C_0	heat capacity of air, $kJ/(g \cdot °C)$
C_S	smoke concentration, g/m^3
C(t)	experimental concentration of CO with time, ppm
CI	subscript denoting coal ignition
CO_A	CO alarm level, ppm
CO_{MAX}	1-min average maximum level of CO, ppm
D	smoke optical density, m^{-1}
D_{CRIT}	critical smoke optical density (value 0.22 m^{-1}) when visibility is about 3.7 m
d_H	hydraulic diameter of entry, m
H_{BR}	belt-to-roof separation, m
H_C	total heat of combustion of fuel, kJ/g
$(H_C)_{ACTUAL}$	actual heat of combustion ($\eta_C \cdot H_C$), kJ/g
H_{CO}	heat of combustion for CO, kJ/g
h	heat transfer coefficient, $kJ/(m \cdot s \cdot °C)$
k_{CO_2}, k_{CO}	stoichiometric yields of CO_2 and CO, g/g
L	location on belt, m
ℓ	distance from fire, m
$\dot{M}_{AIR}$	average mass flux of air, g/s
M''_{FUEL}	mass per unit of fuel surface, g/m^2
$\dot{M}''_{FUEL}$	mass loss rate per unit of fuel surface area, g/m^2s
$\dot{M}_{FUEL}$, $\dot{M}_{CO}$, $\dot{M}_{CO_2}$	generation rates of fuel, CO, and CO_2, g/s
OE	subscript denoting the stage when belt flame spread has reached end of sample
P_0	perimeter, m
Q	heat release rate, kJ/s, kW, or MW
Q_{BI}, Q_{BFS}	heat release rates at time of belt ignition and belt flame spread, respectively
Q_{COAL}, Q_{SBR}	heat release rates for coal and SBR belts, respectively

Q_{CRIT}	critical heat release rate
Q_{EXIT}	heat release rate at exit
Q_{FIRE}	heat release rate of fire
Q_{MAX}	maximum heat release rate
Q_{OE}	heat release rate at time flames reach end of belting
Q_{TOTAL}	total heat release rate
S_{TOTAL}	total burning surface area, m^2
T	subscript denoting local temperature, °C
T_0	ambient temperature, °C
T_{EXIT}	tunnel exit air temperature
T_{MAX}	maximum temperature
t	time, s or min
$(t_A)_{CO}$, $(t_A)_D$, $(t_A)_T$	times from start of coalbed heating until detection alarm levels at 305 m (see reference 3) for CO, smoke (D), or thermal (T) rises, respectively
t_{BI}, t_{BFS}, t_{CI}, t_T, t_{OE}	times for various events referenced to start of heating the coal pile with electrical heaters
t_{CRIT}	time when hazard events such as optical obscuration, CO levels, or thermal levels become critical to health and compromise escape
t_{EXTING}	time available to extinguish or control a belt flame spread once the fire is detected
t_{INCAP}	time to CO incapacitation based on an exposed dose rate of 36,500 ppm•min and a 233-ppm threshold value
t_{MAX}, t_{MIN}	times for maximum and minimum values, respectively
t_s	time for visible smoke from heated coal pile, referenced to start of heating time
V_0	average local airflow velocity, m/s
V_e	average tunnel exit airflow velocity, m/s
V_f	average flame spread rate, cm/s
W	width of belt sample or wood roof, m
X_c	carbon mass fraction, grams of carbon per gram of fuel
Y_{CO}, Y_S	CO or smoke yields, respectively, in grams of product per gram of fuel
α_{COAL}, α_{SBR}	initial fire growth-rate parameters of coal and SBR belts, respectively, kW/min
α_{FS}	fire growth rate during flame spread, kW/min
β	factor describing number of burning surfaces (1 for belt alone; 2 for belt and wood roof), dimensionless
γ	convective heat transfer parameter, m^{-1}
ΔCO, ΔCO_2	CO and CO_2 produced by fire, ppm

ΔO_2	O_2 consumed by fire, ppm
ΔT	temperature increase, °C
ΔT_{AV}	average temperature increase above ambient temperature, °C
Δt_{EXPTL}	experimental elapsed time from belt ignition to start of flame spread
Δt_{FS}	elapsed time during flame spread
Δt_{PRED}	predicted elapsed time from belt ignition to start of flame spread
Δt_x	elapsed time from coal ignition until sensor alarm (offset by 14.25 min)
δt_i	elapsed time between experimental sampling periods
η_C	combustion efficiency, dimensionless
η_F	fuel efficiency, dimensionless
η_{FUEL}	fraction of total fuel mass consumed
ξ	specific smoke extinction coefficient, m^2/g
ρ	density of material, g/m^3
ρ_0	density of air, g/m^3

Abbreviations

diam	diameter
FHP	fire hazard parameter (Q_{FIRE}/V_0A_0), kJ/m^3
HRR	heat release rate, or fire size, W or MW
ID	inside diameter
OD	outside diameter
PTHS	point-type heat sensor
R11	styrene-butadiene rubber belt, three-ply construction, 11 mm thick, 1.07 m wide
SBR	styrene-butadiene rubber

APPENDIX B.—HEAT RELEASE RATES

The heat release rates were calculated by three different methods, using measurements of (1) the CO and CO_2 produced, (2) the amount of O_2 used, and (3) the temperature rise of the tunnel exit gases. When calculated on the basis of gas data, the resultant heat release rate is said to be the total, or actual, heat release rate (Q_{TOTAL}).

The heat release rates with calculation errors because of the use of a constant average linear airflow (V_e) were compared with heat release rates calculated by continuous measurements of mass flows during several fire tests. All three methods depend on the average gaseous mass flow (grams per second of constituents, e.g., CO, CO_2, O_2, or N_2) at the tunnel exit; however, only the linear airflow is measured by an anemometer. Nine bidirectional flow probes near the gas-sampling probe were used in several fire tests to measure the tunnel exit gas velocities and temperatures across the exit plane and to allow estimates of the gaseous mass flow. The 1-min averaged peak heat release rates, assuming a constant exit velocity, were about 10% lower than the peak fire sizes based on mass measurements up to about 6 MW at a nominal 1.0-m/s airflow. The percentage errors were smaller at higher airflows, possibly because of increased turbulence and smaller fluctuations in the gas composition and temperatures. The assumption of constant linear exit velocity during these tests under these fuel-lean conditions did not introduce significant errors (less than 10%). Corrections at the lowest airflows, when air reversals and exit gas dilutions by fresh ambient air are most likely, were not needed since these fire tests were performed on calm days when the prevailing winds did not force air into the tunnel exit.

CALCULATION OF TOTAL HEAT RELEASED USING COMBUSTION GASES CO AND CO_2

The first method requires the total heat of combustion and the mass fraction of carbon in the fuel as well as the mass of CO and CO_2 generated per second. The total heat release rate in kilowatts using the CO and CO_2 produced can be calculated from

$$Q_{TOTAL} = \left[\frac{H_C}{k_{CO_2}}\right] \times \dot{M}_{CO_2} + \left[\frac{H_C - k_{CO} H_{CO}}{k_{CO}}\right] \times \dot{M}_{CO}, \qquad \text{(B-1)}$$

where H_C = total (net) heat of combustion of the fuel, kJ/g,

H_{CO} = heat of combustion of CO, 10.1 kJ/g,

k_{CO_2} = stoichiometric yield of CO_2, g/g,

= 3.67 X_c, where X_c is the carbon mass fraction,

k_{CO} = stoichiometric yield of CO, g/g, = 2.33 X_c,

$\dot{M}_{CO_2}$ = generation rate of CO_2 from the fire, g/s,

= $1.97\times10^{-3}\ V_e A_0\ \Delta CO_2$,

and $\dot{M}_{CO}$ = generation rate of CO from the fire, g/s,

= $1.25\times10^{-3}\ V_e A_0\ \Delta CO$,

where V_e = exit air velocity, m/s,

A_0 = entry cross-sectional area, 7.53 m^2,

ΔCO_2 = CO_2 produced by fire, ppm,

and ΔCO = CO produced by fire, ppm.

Substitution of the above parameters (see also table B-1) into equation B-1 gives:

$$Q_{TOTAL} = \left[1.48\times10^{-2}\left[\frac{H_C}{k_{CO_2}}\right]\Delta CO_2 + 9.41\times10^{-3}\left[\frac{H_C - k_{CO} H_{CO}}{k_{CO}}\right]\Delta CO\right] \times V_e. \qquad \text{(B-2)}$$

Table B-1.—Values of parameters for combustibles used in experiments

Combustible	H_C, kJ/g	X_C, g/g	k_{CO_2}, g/g	k_{CO}, g/g
Pittsburgh coal 1	25.1	0.601	2.21	1.40
Pittsburgh coal 2	30.9	0.743	2.73	1.73
Sewickley coal	30.0	0.712	2.61	1.66
Belt 1	28.7	0.638	2.34	1.49
Belt 2	27.3	0.623	2.29	1.45
Red oak planks	25.8	0.429	1.57	1.00
Hardwood timbers	27.4	0.452	1.66	1.05

CALCULATION OF TOTAL HEAT RELEASED USING OXYGEN CONSUMED

The second method assumes a constant heat release of 13.1 kJ/g of oxygen consumed. This value is an average based on the combustion of various polymeric and natural carbonaceous materials in sufficient oxygen, at least about 12% to 16% in air, and is described in references 12 and 13. The total heat release rate in kilowatts can be calculated from

$$Q_{TOTAL} = 13.1 \text{ kJ/g} \times \dot{M}_{O_2}, \qquad \text{(B-3)}$$

where $\dot{M}_{O_2}$ is the oxygen consumption rate (grams per second) from fire. The oxygen consumption rate is given by

$$\dot{M}_{O_2} = 1.43\times10^{-3} V_e A_0 \Delta O_2, \qquad \text{(B-4)}$$

where ΔO_2 is the oxygen used in parts per million. Equation B-3 becomes, upon substitution of equation B-4 and the fixed parameters,

$$Q_{TOTAL} = 0.141 V_e \Delta O_2, \text{ kW}. \qquad \text{(B-5)}$$

CALCULATION OF HEAT RELEASED USING EXIT GAS TEMPERATURES

The third method assumes that the heat produced by combustion is used to raise the tunnel exit air temperature (T_{EXIT}) above ambient temperature (T_0) and that energy losses to the surrounding walls or steel belt support structure can be neglected. This heat release rate will typically be lower than that calculated by the other two methods and can be calculated from

$$Q_{TOTAL} = C_0 \rho_0 V_e A_0 \Delta T, \qquad \text{(B-6)}$$

where C_0 = heat capacity of air, 1.088×10^{-3} kJ/(g•°C),

ρ_0 = density of air, 1,200 g/m^3,

and $\Delta T = T_{EXIT} - T_0$, °C.

Substitution of these values into equation B-6 gives

$$Q_{EXIT} = 9.83 V_e \Delta T. \qquad \text{(B-7)}$$

Only heat release rates calculated by method 1 were used in this report because of this method's high sensitivity during the early heating stages when the other two method's results are at background levels. The heat release rates by all three methods agreed with each other. However, method 3 gave the lowest values, as expected, because of uncorrected heat losses to the surroundings.

APPENDIX C.—LIMITS ON HEAT RELEASE RATES

The measured growth rates for heat release lead to large heat release rates when extrapolated to long time periods. There are, however, at least two limitations on the growth rates for belt and wood roof fires that must be considered in a ventilated tunnel: the limits imposed by the amounts of fuel and of oxygen that are available for combustion.

FUEL CONSUMPTION LIMITATION

The limiting upper bound on the heat release rate due to fuel limitation may be calculated from the total mass flux of fuel (grams per square meter per second) multiplied by the total burning area (S_{TOTAL}, in square meters). The burning fuel is consumed at a rate dependent on the sample configuration (thickness, size, orientation, energy losses to surroundings, etc.), local oxygen availability, the radiant energy impinging on its surface, the local gas velocity and temperature, and especially the nature of the fuel. The fuel consumption limitation can be estimated from the total burning area for this simplified concurrent, flow-assisted flame spread as follows.

If the flame is spreading at a steady average rate V_f, the final position L to which the flame front has moved can be calculated during the time t that it takes to burn through the belt. An initial position L_0 at some reference time t_0 is chosen such that after time t the fire has just burned out. The total burning surface area (S_{TOTAL}) can then be calculated from the following equation:

$$S_{TOTAL} = \beta\ W\ (L - L_0) = \beta\ W\ V_f\ (t - t_0), \quad \text{(C-1)}$$

where W is the width of the belting or wood roof (1.07 m) and the factor ß is used to describe the number of burning surfaces (neglecting burning on the back surfaces); ß equals 2 for both the belt and the wood roof, and ß equals 1 for the belt alone.

The maximum burning surface can be estimated, and thus also its maximum heat release rate or fuel-limiting value, as follows. The belt and wood roof contain a fixed mass of fuel per unit of surface area (M''_{SBR} and M''_{WOOD}, respectively, where the symbol, ″, refers to a surface-related parameter). This mass of fuel per unit area is linearly related to the fuel thickness. If a constant average value for the mass flux ($\dot{M}''_{FUEL}$) is assumed over a time interval, from t to t_0, and η_{FUEL} is the fraction of the total fuel mass consumed during the time period, then the total mass flux of fuel per unit surface area will be given by

$$\dot{M}''_{FUEL} = \frac{(\dot{M}''_{SBR} + \dot{M}''_{WOOD})\ \eta_{FUEL}}{t - t_0}. \quad \text{(C-2)}$$

The fuel-limited heat release rate (Q^{LIMIT}_{FUEL}) is the product of mass flux, fuel surface area, and actual heat of combustion as

$$Q^{LIMIT}_{FUEL} = \dot{M}''_{FUEL} \times S_{TOTAL} \times (H_C)_{ACTUAL}. \quad \text{(C-3)}$$

$(H_C)_{ACTUAL}$ can be calculated from the combustion efficiency (η_C) and the net heat of combustion (H_C) by the relation

$$(H_C)_{ACTUAL} = \eta_C \cdot H_C. \quad \text{(C-4)}$$

Substitution of the total surface area (equation C-1), the mass flux (equation C-2), and the actual heat of combustion (equation C-4) into equation C-3 gives

$$Q^{LIMIT}_{FUEL} \approx 2\,W\,\eta_{FUEL}\,(M''_{SBR} + M''_{WOOD})\,\eta_C\,H_C\,V_f. \quad \text{(C-5)}$$

Assuming reasonable parameter values of η_{FUEL} = 0.6, M''_{SBR} = 14.0 kg/m², M''_{WOOD} = 21.1 kg/m², and W = 1.07 m, the heat release rate in megawatts at the fuel consumption limit (equation C-5) becomes

$$Q^{LIMIT}_{FUEL} = 0.45\ \eta_C\ H_C\ V_f, \quad \text{(C-6)}$$

where the velocity units for the average flame front are centimeters per second, and both belt and wood surfaces are included. For belting only, the expression is

$$Q^{LIMIT}_{FUEL} = 0.090\ \eta_C\ H_C\ V_f. \quad \text{(C-7)}$$

Equations C-6 and C-7 represent the fuel consumption limitations on the heat release rate (megawatts) for both belt and roof, and for belt only, respectively, as functions of the combustion efficiency and flame front velocities (centimeters per second).

OXYGEN AVAILABILITY LIMITATION

A stoichiometric ratio of fuel to air is that ratio calculated on the basis of conversion of fuel and oxygen to

the products CO_2 and water (H_2O). If there is an excess of air available for combustion, then the combustion process is said to be fuel-lean. If there is an excess of fuel available for combustion, then the combustion process is said to be fuel-rich. The stoichiometric fuel-to-air mass ratio is 0.11 for SBR belting and 0.22 for wood. Assuming an average value of 0.12, the stoichiometric heat release rate will occur when

$$\frac{\dot{M}_{FUEL}}{\dot{M}_{AIR}} = 0.12. \qquad \text{(C-8)}$$

The $\dot{M}_{FUEL}$ is the average mass flux times the surface area, and $\dot{M}_{AIR}$ is the average mass flux of air, which is equal to $\rho_0 V_0 A_0$. The heat release rate can be expressed by

$$Q_{AIR}^{LIMIT} = 0.12\ \rho_0\ V_0\ A_0\ \eta_C\ H_C. \qquad \text{(C-9)}$$

Substituting for ρ_0 and A_0, the heat release rate in megawatts at the stoichiometric limit (equation C-9) becomes

$$Q_{AIR}^{LIMIT} = 1.084\ V_0\ \eta_C\ H_C. \qquad \text{(C-10)}$$

Heat release rates at both the fuel limit and stoichiometric limit depend upon the combustion efficiency η_C, which was determined experimentally as follows: First, the heat release rates (Q_{OE}) were determined using appendix equation B-2 at the time the flame front reaches the end of the belting. At this time the total surface area is assumed to be burning, and S_{TOTAL} equals 13.0 m^2 for the belt and roof, or 6.5 m^2 for the belt only. The mass fluxes were determined by dividing the mass of belting per unit surface area by the time of burning obtained from thermocouple data. The combustion efficiency is then given by

$$\eta_C = \frac{Q_{OE}}{\dot{M}''_{FUEL} \cdot S_{TOTAL} \cdot H_C}. \qquad \text{(C-11)}$$

The data and resultant values of η_C are shown in table C-1. It was also found that a best fit of the average values of η_C at each velocity yielded the following expression:

$$\eta_C = 1 - e^{-0.24\ V_0}. \qquad \text{(C-12)}$$

If equation C-6 is set equal to equation C-10, then a limit flame front velocity can be determined, which represents the flame front velocity necessary for the fires to burn at the stoichiometric-limited heat release rates. This value is given by

$$V_f = 2.4\ V_0. \qquad \text{(C-13)}$$

Table C-1.—Combustion efficiency from mass flux estimates

Test	V_0, m/s	Q_{OE}, MW	$(\dot{M}''_{FUEL})_{MEAS}$, g/m²s	η_C
LOW AIRFLOW				
3	0.77	0.45	NA	NA
4	0.75	0.57	13.1	0.123
12	0.74	1.23	19.9	0.174
14	0.62	0.82	13.7	0.166
16	0.75	1.45	20.6	0.199
Av	0.73±0.06	0.90±0.42	16.8±4.0	0.165
MEDIUM AIRFLOW				
7	1.5	1.90	16	0.334
15	1.7	2.25	22.2	0.286
Av	1.6±0.1	2.08±0.25	19.1±4.4	0.310
HIGH AIRFLOW				
2	4.5	3.60	[1]27.6	0.699
5	3.8	4.37	NA	NA
6	4.0	4.51	[1]30.7	0.788
10	3.9	7.77	45.6	0.480
13	4.0	7.90	39.5	0.565
Av	4.0±0.3	5.63±2.04	35.9±8.2	0.633

Av Arithmetic average and standard deviation.
NA Not available.
[1]Little roof contribution at time when belt flame reached end of sample.

Flames that spread at a rate less than this estimated value can be expected to burn on the fuel-lean side, and flames that spread faster will eventually become fuel-rich. Table C-2 summarizes all the experimental belt and roof flame spreads along with their average values. Table C-3 shows the results of the calculations for fuel- and stoichiometric-limited heat release rates from equations C-7 and C-10, and the experimentally measured maximum heat release values.

From equation C-13, the limit flame front velocities at 0.76-, 1.6-, and 4.1-m/s air velocities are 1.8, 3.8, and 9.8 cm/s, respectively. From table C-2, only two tests (14 and 16) at an air velocity of 0.76 m/s resulted in flame front velocities in excess of the limit value. From table C-3, one of these tests (16) had a maximum heat release rate in excess of the stoichiometric limit value, indicating a fuel-rich condition.

Table C-2.—Belt and roof flame spread rates and average flame spread rates

Test	H_{BR}, m	Flame spread, cm/s		
		Belt	Roof	V_f[1]
	LOW AIRFLOW			
3	1.4	0.61	0.51	0.56
4	1.4	0.61	0.86	0.74
12	1.4	0.76	1.5	1.13
14	0.8	13.2	15.2	14.2
16	0.8	11.7	5.6	8.65
	MEDIUM AIRFLOW			
1	1.4	0.91	3.6	2.26
7	1.4	1.1	[2]−0.41	1.07
15	0.8	2.0	4.1	3.05
	HIGH AIRFLOW			
2	1.4	0.76	1.0	0.88
5	1.4	0.71	[3]NP	0.71
6	1.4	0.66	[3]NP	0.66
10	1.4	0.86	1.0	0.93
13	0.8	2.0	6.1	4.05

[1]Average of top belt and wood roof flame spreads.
[2]Flashing flame was extinguished and was followed by a final flame, which started at about 3 m and moved upstream.
[3]Nonpropagating flames flashed over the surface and slightly charred the roof.

Table C-3.—Local airflow over belting, calculated limited fuel and stoichiometric heat releases, and measured maximum heat release rates

Test	V_0, m/s	Q_{FUEL}^{LIMIT}, MW	Q_{AIR}^{LIMIT}, MW	Q_{MAX}^{MEAS}, MW
		LOW AIRFLOW		
3	0.76	1.15	3.76	0.63
4	0.76	1.12	2.77	2.40
12	0.76	2.39	3.91	3.40
14	0.76	29.0	3.73	2.50
16	0.76	21.0	4.45	9.70
		MEDIUM AIRFLOW		
1	1.63	8.92	15.6	2.20
7	1.52	4.39	15.0	3.30
15	1.68	10.7	14.2	6.20
		HIGH AIRFLOW		
2	4.52	6.53	93.5	3.70
5	3.76	5.18	66.1	4.95
6	4.06	6.39	94.7	5.65
10	3.91	5.54	55.5	8.70
13	4.01	28.3	67.1	14.5

If the average flame spread rates are used, then it is possible to estimate the fuel-limited heat release rates and the air-limited heat release rates for both large and small belt-to-roof separations. These rates are shown in figure C-1 and compared with the 1-min average peak values. Analysis of figure C-1 indicates two main effects:

1. For rapid flame spread rates (tests 14 and 16, table C-3), at the lowest airflow (V_0 = 0.76 m/s) and the low belt-to-roof separation (H_{BR} = 0.8 m), the fuel-limited heat release rate exceeds the air-limited heat release rate. This means that the air limit represents the major constraint on the value of the heat release rate. It also means that the fire spread has the potential to traverse into the region of fuel-rich combustion before adjusting to the limited air supply. The danger of this is that the rate of CO production increases markedly in the fuel-rich combustion region (i.e., the area between the fuel and air limit curves in figure C-1). Test 16 did produce a peak heat release rate (HRR) in excess of the air limit value with a corresponding increase in CO production (test 16; maximum HRR = 9.7 MW; B_{CO} = 13.3). For rapid flame spread rates, it is also clear that the tests were limited by the quantity of fuel available.

2. For slower flame spread rates and the high belt-to-roof separation (H_{BR} = 1.4 m), limiting heat release rates are due to the fuel available and pose the limiting constraint. In these cases, the flame spread rate is sufficiently slow so that burnout of the trailing edge of the flame occurs, thus limiting the surface area available for combustion. For these tests, there was adequate fuel available to begin to approach the fuel limited value, as shown by the average maximum experimental values in figure C-1 for two belt-to-roof separation distances and at three air velocities.

For fires in which there is typically more than sufficient tunnel air to burn the fuel at the lean side of the stoichiometric ratio, local air-fuel concentrations in the fire may still be occurring at the stoichiometric ratio. The flames tend to entrain the air at the rate necessary to sustain the combustion at or near the stoichiometric air-fuel ratio. For fires with heat release rates greater than the stoichiometric limit, fuel-rich combustion definitely occurs, owing to the fact that external factors (e.g., ventilation) limit the quantity of air available for entrainment.

The measured maximum heat release rates using appendix B equation B-2 are given in column 5 of table C-3. The calculated heat release rate limits at both the fuel limit and the oxygen consumption limit are shown in columns 3 and 4, respectively. An average net heat of combustion of 27.3 kJ/g and the measured air velocity parameters were used in the calculations as described above.

Figure C-1

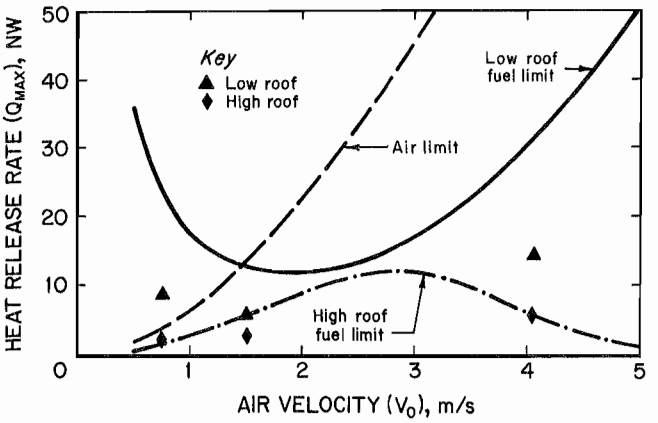

Estimated maximum heat release rates for belt fires that are low roof and high roof fuel-limited and air-limited. The experimental maximum values at 0.8- and 1.4-m belt-to-roof separations are given at three air velocities.

In table C-3, the fuel limit (column 3) provides the governing restraint on the maximum heat release rate for all the tests, except tests 14 and 16, which are air limited (column 4). The lowest value for the upper bounds gives the maximum attainable value theoretically possible for these tests. Only the peak measured values (column 5) in tests 5, 6, and 10 approached their maximum values of heat release rate and were, of course, fuel limited. For one high-air-velocity test (test 13), the measured maximum heat release rate is only 51% of the limit value based on fuel consumption. For all the tests at the lowest air velocity and the three tests at the intermediate velocity (tests 1, 7, and 15), the maximum measured heat release rates averaged only 27% of the fuel-limited values. This implies that the maximum heat release rate was limited by the fuel available and perhaps three to four times as much fuel would be needed to achieve the true limit conditions for this tunnel configuration.

For tests 16 and 14 at a belt-to-roof separation of 0.8 m, the fuel limits are 5 and 10 times higher than the air limits, respectively. These two tests could become fuel rich because of the rapid flame spread rates. The resulting fires would burn on the rich side of the stoichiometric ratio before experiencing the effects of reduced oxygen. For combustion on the rich side, the production of CO can increase by as much as a factor of 10, thus increasing the CO level to values that may be lethal in several breaths.

Figure C-2 shows the regions where it is probable that fires will become fuel rich, based on rates of belt and wood roof flame spread and the ventilating air velocity. The upper region (1) represents those flame spread rates

Figure C-2

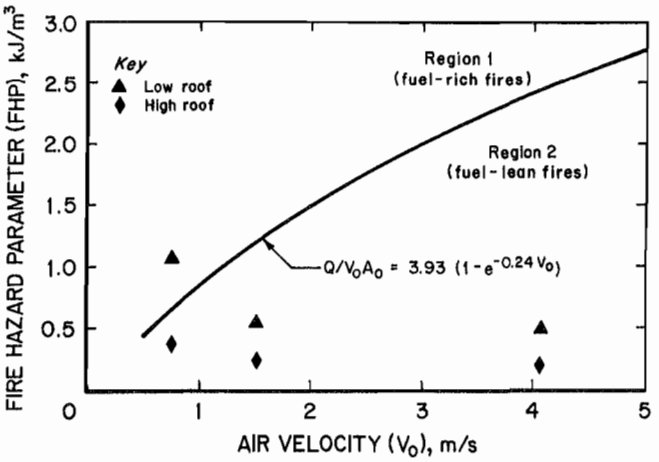

Fire hazard parameter versus air velocity showing the regions where fuel-rich and fuel-lean fires are likely to occur. Experimental values are shown for two belt-to-roof separations at three velocities. The estimated air-limited curve separates the two regions.

Figure C-3

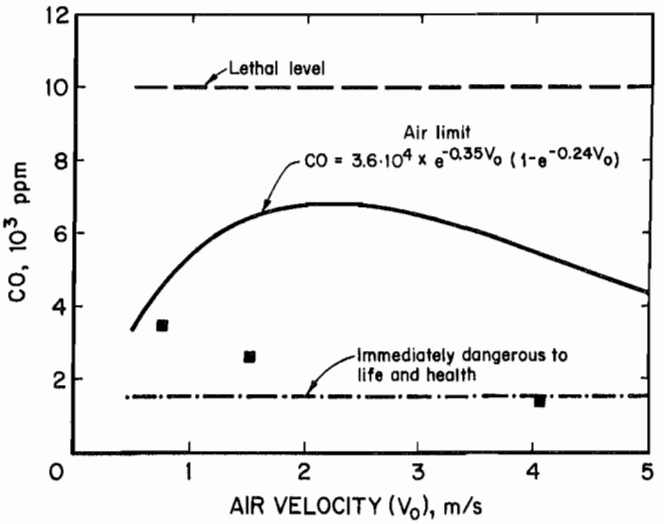

CO concentration curve for calculated air limit at various air velocities. Experimental maximum values, immediately dangerous to life and health, and lethal level are shown.

that have a high probability of producing fuel-rich fires, while the lower region (2) represents spread rates that have a low probability of producing fuel-rich fires at the given air velocities. Using equation C-10 for the air limit, the curve separating the two regions as a function of the velocity is written in terms of the fire hazard parameter (FHP) as

$$FHP_{LIMIT}^{AIR} \equiv \frac{Q_{AIR}^{LIMIT}}{V_0 A_0} = 3.93 \times 10^3 \left(1 - e^{-0.24 V_0}\right). \quad \text{(C-14)}$$

Using the average CO production constants from table 6 in the main text, it is found that B_{CO} varies with air velocity according to the expression

$$B_{CO} = 9.1\ e^{-0.35\ V_0}. \quad \text{(C-15)}$$

The levels of CO that would result at the stoichiometric-limited heat release rate can be estimated from the product of equations C-14 and C-15. The result is given by

$$CO_{ppm} = 3.6 \times 10^4 \cdot e^{-0.35\ V_0} \left(1 - e^{-0.24 V_0}\right), \quad \text{(C-16)}$$

and plotted in figure C-3 along with the incapacitation 30-min dose at 1,500 ppm and the lethal 10-min level of 10,000 ppm. Near lethal concentrations of CO, 5,000 to 7,000 ppm, are approached at air velocities from 1 to 3 m/s, respectively, even for fires that are not burning on the fuel-rich side of the stoichiometric fuel-to-air ratio.

Fuel-rich fires represent a much greater fire hazard because of the increase in CO production that occurs. The analysis presented above for this belt and roof configuration (figure 1 in the main text) demonstrates the possibility of fuel-rich fires in conveyor belt entries. The magnitude of the fire hazard can be quantified using the FHP, which is defined as the heat release rate divided by the product of the air velocity times the cross-sectional gallery area. In assessing the magnitude of the hazard, time is a critical component, and the stoichiometric limit on the heat release rate is a convenient reference point since for larger fires, fuel-rich combustion begins to occur. One way to assess the times to reach this stoichiometric limit is through the use of the fire growth rate measured during flame spread. A second way to assess these times is through the use of the measured flame front velocities. This latter approach also provides insight into the surface area that must be involved in order to produce this limit heat release rate.

Table C-4 presents the data for fire growth rates measured during the stage of flame spread (α_{FS}) in terms of the heat release rates measured at the onset of flame spread (Q_{BFS}), the heat release rate measured when flames reach the end of the belting and roof (Q_{OE}), and the time that elapses during this stage of fire growth (Δt_{FS}). The

fire growth rates are given in column 6. Note that at the lower belt-to-roof distance of 0.8 m, the fire growth rates increase dramatically in a manner similar to the flame front velocities.

From table 4 in the main text, the ratio of heat release rate to ventilation air velocity at the onset of belt flame spread has an average value of 394, or in terms of the FHP value, 52.0 kJ/m^3. The FHP value at the stoichiometric limit of heat release rate is given by equation C-14.

The average times to reach this stoichiometric limit are given by

$$t_{LIMIT}^{AIR} = \frac{V_0 A_0}{\alpha_{FS}} (FHP_{LIMIT}^{AIR} - FHP_{BFS}). \quad (C\text{-}17)$$

The average flame front velocities may also be used to determine these average times from the expression

$$t_{LIMIT}^{AIR} = \frac{V_0 A_0}{60 \eta_C \dot{M}''_{FUEL} H_C (V_f)_{AV}} \left(FHP_{LIMIT}^{AIR} - FHP_{BFS} \right). \quad (C\text{-}18)$$

Table C-4.—Elapsed times between start of belt flame spread and time belt flame reaches sample end, heat release rates at the respective times, and fire growth rate during elapsed time period

Test	H_{BR}, m	Δt_{FS}, min	Q_{OE}, kW	Q_{BFS}, kW	α_{FS},[1] kW/min
			LOW AIRFLOW		
3	1.4	14	450	170	20.0
4	1.4	13	570	270	23.1
12	1.4	11	1,230	490	67.3
Av	1.4	13	750±420	310±160	37±27
14	0.8	0.5	820	490	660
16	0.8	1	1,450	380	1,070
Av	0.8	1	1,140±450	440±78	870±290
			MEDIUM AIRFLOW		
7	1.4	7	1,900	450	207
15	0.8	3	2,250	720	510
			HIGH AIRFLOW		
2	1.4	10	3,600	1,470	213
5	1.4	8	4,370	1,670	338
6	1.4	8	4,510	2,120	299
10	1.4	9	7,770	710	784
Av	1.4	9±1	5,060±1,850	1,490±590	409±260
13	0.8	4	7,900	960	1,735

Av Arithmetic average and standard deviation.
[1]Belt fire growth rate from time of belt ignition until start of belt flame spread. Calculated by $\alpha_{FS} = (Q_{OE} - Q_{BFS})/\Delta t_{FS}$.

Table C-5 compares the average times to reach the stoichiometric limit for heat release rate using the two above equations for both roof-to-belt separations. From table C-5, the two methods of computing the time to reach the stoichiometric limit on heat release rate compare favorably. Column 5 of table C-5 represents the length of belting needed to achieve this limit on the heat release rate. Inspection of equations C-17 and C-18 indicate that the fire growth rate can be expressed by

$$\alpha_{FS} = 60 \eta_C \dot{M}''_{FUEL} H_C (V_f). \quad (C\text{-}19)$$

A slower belt flame spread rate and/or smaller mass flux rate and/or lower heat of combustion can thus be shown to directly affect the fire growth rate α_{FS}. Slower fire growth rates can readily be achieved by belts that do not propagate flame spread (e.g., $V_f = 0$).

Table C-5.—Times to achieve air-limited stoichiometric heat release rate from average fire growth rates and flame spread rates and minimum length of belt sample required at various airflows and belt-to-roof separations

v_0, m/s	H_{BR}, m	t_{LIMIT},[1] min		L_{MIN},[2] m
		Equation C-17	Equation C-18	
0.76	1.4	94	91	45
	0.8	4	6.5	45
1.6	1.4	70	63	87
	0.8	28	48	87
4.1	1.4	182	217	121
	0.8	43	50	121

[1]Average time to reach air limited stoichiometric heat release rate calculated by equation C-17 or C-18.
[2]Average minimum length of belt to achieve air-limited stoichiometric heat release rate for 1-m-wide belt sample.

APPENDIX D.—RELATIONSHIPS BETWEEN PRODUCTION CONSTANTS FOR CO AND SMOKE AND THEIR YIELDS

The production constant for CO (B_{CO}) is defined from the equation

$$CO_{ppm} = B_{CO} \cdot (Q/V_0A_0), \qquad (D\text{-}1)$$

where CO = measured concentration of CO, ppm,

Q = measured values of heat release rate, kW,

V_0 = air velocity, m/s,

and A_0 = cross-sectional area of tunnel, m^2.

The concentration of CO is also related to the yield of CO (Y_{CO}), fuel (M_{FUEL}, grams per second) by the expression

$$CO_{ppm} = (800 \cdot Y_{CO} \cdot \dot{M}_{FUEL})/V_0A_0, \qquad (D\text{-}2)$$

where 800 is a constant with units of parts per million per cubic meter per gram used to convert the CO mass concentration to parts per million.

The mass loss rate of the fuel is related to the heat release rate (Q) by the expression

$$\dot{M}_{FUEL} = Q/\eta_C H_C, \qquad (D\text{-}3)$$

where H_C = total heat of combustion of the fuel, kJ/g,

and η_C = combustion efficiency.

Combining equations D-1 through D-3 results in the following expression for the yield of CO as a function of the CO production constant:

$$Y_{CO} = 1.25\times10^{-3} \cdot B_{CO} \cdot \eta_C \cdot H_C. \qquad (D\text{-}4)$$

The smoke optical density (B_D, inverse meters) is related to the concentration of CO (parts per million), see equation 9 in the main text, by the expression

$$B_D = 0.011 \cdot B_{CO}. \qquad (D\text{-}5)$$

The smoke optical density is defined by the expression

$$B_D = 0.65 \cdot \xi \cdot C_S, \qquad (D\text{-}6)$$

where the parameter ξ is called the specific extinction coefficient with units of square meters per gram, and C_S is the smoke concentration (grams per cubic meter).

As for CO, the smoke concentration C_S is related to the smoke yield Y_S (grams per gram) by the expression

$$C_S = (Y_S \cdot \dot{M}_{FUEL})/(V_0A_0). \qquad (D\text{-}7)$$

Combining equations D-2 through D-7 yields the following expression for the smoke yield:

$$Y_S = Y_{CO} \cdot 13.5/\xi. \qquad (D\text{-}8)$$

The literature data for ξ suggest values of 7.9 (*14*)[1] or 5.1 (*15*). Assuming an average value of 6.5 for ξ, then

$$Y_S = 2.1 \cdot Y_{CO}. \qquad (D\text{-}9)$$

Equations D-4 and D-9 can then be used to estimate the yields of CO and smoke, respectively, from the measured values of B_{CO} (table 6 in the main text) and the measured values of η_C from table C-1. The result is shown in table D-1. These data are in good agreement with the yields reported (*15*) for a range of synthetic polymers. The factor 2.1 in equation D-9 is in excellent agreement with the value of 2.3 reported (*7*).

[1]Italic numbers in parentheses refer to items in the list of references preceding the appendixes.

Table D-1.—Estimates of CO and smoke yields

Test	B_{CO}	η_C	Y_{CO}, g/g	Y_S, g/g
		LOW AIRFLOW		
3	6.1	0.165[1]	0.035	0.074
4	6.4	0.123	0.028	0.058
12	4.3	0.174	0.026	0.055
14	7.6	0.166	0.044	0.093
16	13.3	0.199	0.093	0.195
Av	7.5±3.4	0.165±0.027	0.045±0.028	0.095±0.058
		MEDIUM AIRFLOW		
7	4.1	0.334	0.048	0.101
15	7.3	0.286	0.073	0.154
Av	5.7±2.3	0.310±0.034	0.061±0.018	0.128±0.037
		HIGH AIRFLOW		
2	2.9	0.699	0.071	0.149
5	3.7	0.633	0.082	0.172
6	4.1	0.788	0.113	0.238
10	3.1	0.480	0.052	0.109
13	2.7	0.565	0.053	0.112
Av	3.3±0.6	0.633±0.119	0.074±0.025	0.156±0.053

Av Arithmetic average and standard deviation.
[1]Average value of η_C from table C-1.

APPENDIX E.—SUMMARY OF SIGNIFICANT EVENTS AND SELECTED PARAMETERS

The times from the start of heating the coalbed until the occurrence of significant events are summarized in table E-1 for all pertinent tests at 0.76-, 1.6-, and 4.1-m/s airflows. The event times are averaged for several tests over the total airflow range where it is appropriate and at the given airflows. Their standard deviations are also given unless there was only one test. The $(t_A)_D$, $(t_A)_{CO}$, and $(t_A)_T$ average alarm times for smoke, CO, and temperature, respectively, are measured and based on the criteria of reference 3 for detectors spaced at intervals of 305 m for the gas sensors and at about a 6-m interval for the thermal sensor.

The maximum temperatures, CO levels and heat release rates are averaged over a time interval of 1 min in table E-2. The belt and wood roof flame spreads and heat release values are averaged during the flame travel over the last few meters of sample. The α_{COAL} and α_{SBR} values are independent of H_{BR} levels during this initial fire growth stage.

Table E-1.—Summary of events at three airflows

Event time, min	V_0 = 0.76 m/s	V_0 = 1.6 m/s	V_0 = 4.1 m/s	Av values[1]
t_S	62±5	70±5	73±6	68±7
$(t_A)_D$	108±16	121±16	127±26	119±20
$(t_A)_{CO}$	125±13	134±20	133±26	131±20
t_{CI}	137±10	140±16	127±15	135±14
t_{BI}	155±13	157±16	161±27	158±19
t_{BFS}	221±20	173±16	170±27	200±33
$(t_A)_T$	>201	189±22	>182	>201
t_{OE}	242±11	179±18	193±35	205±33

[1]Av values independent of airflow V_0 for all 16 tests.

Table E-2.—Maximum and average values of selected parameters at three airflows and two belt-to-roof separations

Parameter	V_0 = 0.76 m/s	V_0 = 1.6 m/s	V_0 = 4.1 m/s
T_{MAX} for roof at 0.0 m,[1] °C:			
H_{BR} = 1.4 m	750±40	610	20±6
H_{BR} = 0.8 m	800±100	640	24
T_{MAX} for roof at 27.4 m,[2] °C:			
H_{BR} = 1.4 m	490±150	480	250±50
H_{BR} = 0.8 m	650±130	520	590
CO_{MAX}, ppm:			
H_{BR} = 1.4 m	1,400±900	1,500	750±200
H_{BR} = 0.8 m	3,500±900	2,600	1,300
Belt flame spread, cm/s:			
H_{BR} = 1.4 m	0.66±0.09	1.0±0.1	0.86
H_{BR} = 0.8 m	12.5±1.1	2.0	2.0
Roof flame spread, cm/s:			
H_{BR} = 1.4 m	1.0±0.5	3.6	1.0
H_{BR} = 0.8 m	10.4±6.7	4.1	6.1
Q_{MAX}, MW:			
H_{BR} = 1.4 m	2.1±1.4	2.8±0.5	5.8±2.1
H_{BR} = 0.8 m	6.1	6.2	15
α_{COAL}, kW/min	2.0	2.9	3.8
α_{SBR}, kW/min	7.1±4.9	20±7	66±30
α_{FS}, kW/min:			
H_{BR} = 1.4 m	37	207	410
H_{BR} = 0.8 m	870	510	1,740

[1]Roof temperature measured at fire gallery entrance (reference 0.0 m) about 2.7 m upwind of coal pile.
[2]Roof temperature at fire gallery exit (position 27.4 m).

INT.BU.OF MINES,PGH.,PA 30153

☆ USGPO 609-012/20,032